Erratum to the Thesis **Implementation and verification of the USGS solute transport code MT3DMS for groundwater heat transport modeling**.

Author: Jozsef Hecht Méndez

Thesis date: August 2008

The numerical code MT3DS is **not** an USGS software as stated in the title and in page 12 of the present thesis.

The developer of MT3DMS is Dr. Chunmiao Zheng. All relevant information about the code can be found at: http://hydro.geo.ua.edu/mt3d/

Tübingen, December 10th, 2008

Implementation and verification of the USGS solute transport code MT3DMS for groundwater heat transport modelling

Jozsef Hecht Méndez

Supervisors
Dr. Philipp Blum
Dr. Peter Bayer

Tübingen, August 2008

I hereby certify that the work presented here
was conducted solely by myself and
with the aid of the references listed.

August, 2008   Jozsef Hecht Méndez

…to my Father (1941-2006)…

ACKNOWLEDGEMENT

TABLE OF CONTENTS

LIST OF FIGURES

LIST OF TABLES

ABSTRACT

The multi-species solute transport model MT3DMS, originally developed for solute transport modelling, is applied to simulate heat transport in porous media. It is shown, how to implement the numerical code for modelling borehole heat exchangers (BHEs) used in shallow geothermal technologies. Moreover, MT3DMS is verified using various analytical solutions and one alternative numerical code: 1) comparing the numerical results with results obtained by three analytical solutions and, 2) comparing the MT3DMS results with an alternative numerical code (SHEMAT; Clauser, 2003).

For the implementation, features related to grid dimensions and discretization at cells, where the energy extraction/injection is located are analyzed. Other issues related to the code capabilities were also studied such as: performance of the various solvers used for the numerical calculations and entering of the macrodispersion coefficient as 2D or 3D arrays. Regarding to the verification, three main test cases are considered based on three hydraulic gradients (conduction dominated, intermediate and convection dominated systems). The numerical results are compared with analytical solutions for 2D and 3D point, line or planar sources. For the verification with SHEMAT, one 2D scenario was modelled (convection dominated).

From the evaluations, it was determined that for heat transport simulation of a single BHE, the model grid size should range from 200 m × 200 m to 500 m × 500 m for 2D and 3D models. For the 3D cases, a minimum of 7 layers or 7 m thickness should be used in order to avoid boundary effects in the z-axis. From the advection solver analysis, it is noticed that the third order ULTIMATE method shows the best matches with the analytical results for three different hydraulic gradients. However, the other solvers show satisfactory matches with the analytical solutions.

Concerning the verification, the MT3DMS results have high match efficiencies with the analytical solutions for all the 2D and 3D test cases. The best approximation was obtained for convection dominated problem ($i = 1.2E-3$) with an efficiency of 0.99. For $i = 0$ (only conduction), the efficiency is 0.96. For intermediate problem ($i = 6.0E-5$), the match between numerical and analytical solution showed an efficiency of 0.92. Regarding the comparison with the numerical code SHEMAT, the MT3DMS results fit well with the SHEMAT results. There was only a slightly temperature difference of 0.4 K within 10 m distance from the source.

1 INTRODUCTION

1.1 Shallow geothermal energy – open and closed systems

According to the directive of the German Association of Engineers (VDI 4640-Richtlinie, 2000), geothermal energy is defined as the form of energy stored as heat below the surface of the solid earth. Down to a depth of about 400 m, shallow geothermal energy is considered, whereas at greater depth, deep geothermal technologies are applied. The temperatures of shallow geothermal applications commonly range between 8 and 25°C (Scholz, written communication), however these values could considerably change depending on the conditions of the specific geological environment.

Shallow geothermal energy is mainly used for heating/cooling of buildings. In recent years, due to the rising energy costs, alternative and ideally regenerative energy resources are gaining attention. Hence, this application shows a rapid increase (Lund et al., 2005). To mine this energy, so-called ground source heat pump (GSHP) systems are employed. There are two main types of GSHP systems: closed systems and open systems (Figure 1). The closed system is composed of a heat pump and a borehole heat exchanger (BHE). In open systems, groundwater is used as the fluid carrying the heat and it is brought directly to the heat pump. In closed systems, the heat is taken from an aquifer through a circulation fluid within the pipes (BHE), which usually contains water and anti-freeze liquids (Diao et al., 2004). In the latter, heat is mined by diffusion. In this process, heat diffuses into GSHP system across the pipes from the outside ground or rock and from the groundwater (Clauser, 2006).
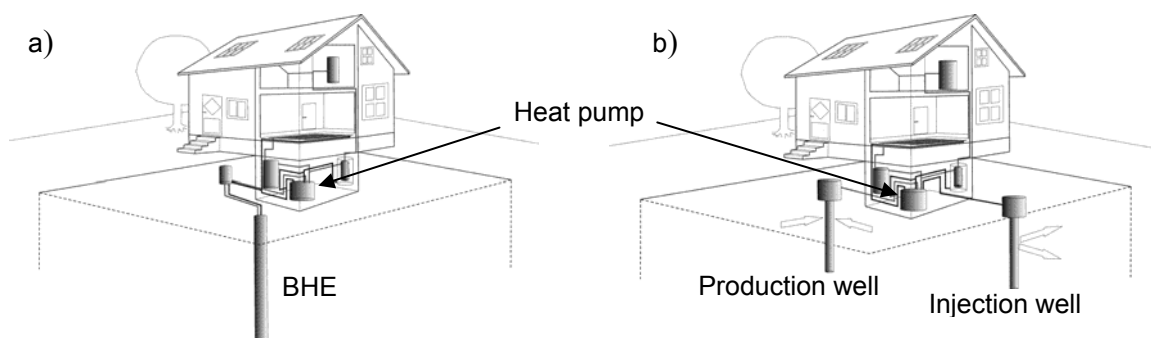
Figure 1. Ground source heat pump systems, a) closed system, b) open system.

1.2 Heat transport simulation

Heat is transported in the ground by two major processes: conduction and convection. Understanding of these processes is required for applying GSHP systems in a shallow geothermal reservoir, for instance an aquifer.

Heat transport mechanisms are mathematically described by partial differential equations (PDEs). These PDEs can be solved by analytical or numerical methods. However, there are problem formulations for which an analytical solution, i.e. a direct solution at the level of mathematical analysis, cannot be found (Holzbecher, 1998). For such problems, computer based implementations of numerical methods are common. Computer based numerical methods are also called numerical simulation or numerical modelling. Numerical simulations are used in various areas of geosciences and engineering disciplines. For example, in hydrogeology, they are applied to solve problems related to groundwater, solute and heat movement. These methods are essential in order to analyze the described transport processes in detail, to reveal parameter sensitivities, to predict future states and simulate the performance of environmental technologies.

Computer based simulations of geothermal systems are common, and by 2000 it had been used at about 100 fields worldwide (e.g. O´Sullivan et al., 2000). Actually, there is a great variety of software for heat simulation, either commercial or open source, such as HST3D (Kipp, 1986), SHEMAT (Clauser, 2003) and FEFLOW (Diersch, 2002). Despite the increasing availability of heat simulation software, codes developed for solute transport simulation still have more capabilities for solving the PDEs related to the transport phenomena. One of these comprehensive numerical codes is MT3DMS developed by Zheng and Wang (1999).

MT3DMS stands for a "Modular 3-Dimensional Transport Multi-Species" model and is part of the United States Geological Survey (USGS) MODFLOW family. Commonly, it is used as a post-processor to simulate solute transport based on a flow field usually calculated by the numerical code MODFLOW. As MODFLOW, it is based on finite differences. MT3DMS has been widely used in contaminant transport problems. A list of these applications can be found on the University of Alabama webpage (groundwater group). Cathomen (2002) applied MT3DMS to calculate the groundwater temperature distribution in a delimited area of the Altach Municipality (Austria). In this work, groundwater flow simulations were performed under the influence of heat extraction wells and heat pumps located within the study area.

Although a description of the adoption of the numerical code to heat transport modelling is presented, this work does not include any rigorous verification of using MT3DMS for heat transport simulation.

1.3 Objectives

Due to the mathematical similarity between the governing equations of solute and heat transport, the numerical code MT3DMS originally designed for solute transport simulation can also be used for heat transport modelling. For this purpose, the analogous parameters included in the partial differential equations of solute and heat transport have to be identified and defined accordingly. Likewise, to confirm the adoption of MT3DMS for heat transport simulation, a verification of the code hast to be performed. By verification, numerical results are compared with analytical solutions for a specific situation or with another numerical code.

Thus, the main objective of this thesis is the implementation and verification of MT3DMS (Version 5.2, Zheng and Wang, 1999) for simulating 2D and 3D heat transport. A recipe will be developed for adopting the software for heat transport modelling and more specific, for simulating and predicting the effect of closed system such as GSHP. The underlying work is part of a team investigation carried out by the geothermal group of the Centre of Applied Geosciences (ZAG). Please note that, a comprehensive investigation with a compendium of available analytical solutions for heat transport modelling is major part of the thesis by Molina (2008) and thus not in the fore of the work presented here.

Adopting MT3DMS for heat transport modeling is appealing due to following features: Firstly, it is a free and continuously maintained FORTRAN code that can be downloaded from the Alabama university webpage (Alabama University, 2007). This enables to change the code for specific applications and if necessary, new subroutines can be included. Secondly, MT3DMS includes three major classes of transport solution techniques (the standard finite-difference method, the particle tracking based Euler-Langrangian methods, and the higher-order finite-volume TVD method) in a single code (Zheng and Wang, 1999). Thirdly, it is compatible with the most common groundwater flow package MODFLOW 2000 (Harbaugh et al., 2000), but it can also used flow fields calculated with other numerical codes. Finally, important descriptive parameters such as longitudinal dispersivity and thermal diffusivity can be defined as 2D or 3D arrays. This feature allows inclusion of heterogeneities in the model. The present work will provide a first comprehensive assessment for using the

numerical code MT3DMS for heat transport modelling and it offers a basic user guide for numerical modelling of borehole heat exchanger in shallow confined aquifers.

1.4 Overview of thesis

In the subsequent paragraphs, the implementation and verification of MT3DMS for heat transport simulation is explained in a straightforward fashion. In the first chapter, we present a brief insight into the state-of-the-art of heat transport simulation practice and the description of the numerical technique (finite differences) used by MT3DMS. In this chapter, the analogy between solute and heat transport governing equations is also described. For the latter, the conforming coefficients and its implementation in MT3DMS are given.

The second chapter deals with the adoption of MT3DMS for heat transport simulations. Following aspects are analyzed: formulation of boundary conditions for a heat extraction borehole (closed systems) used in a confined aquifer; choice of advection solver depending on the groundwater velocity field, discretization at the cells where the energy extraction/injection is applied, inclusion of the macrodispersion coefficient and its effect on the length of the heat plume is also evaluated.

The third chapter contains the verification of applying MT3DMS for heat transport simulation. Both, 2D and 3D cases are considered for a range of hypothetical scenarios with three hydraulic gradients ($i = 0$, $i = 6.0E-5$ and $i = 1.2E-3$). In the first part of this chapter, MT3DMS outputs are compared to results from analytical solutions. In the second part, MT3DMS is compared to an alternative numerical code, the commercially available heat transport program SHEMAT (Clauser, 2003).

In the fourth chapter, a final discussion summarizing the findings from previous chapters is presented, and the upcoming objectives of the geothermal research group regarding to further application of MT3DMS for heat transport modelling.

2 THEORETICAL BACKGROUND

2.1 Heat transport simulation in groundwater

Numerical modelling has become a useful element for planning shallow geothermal technologies. It is used in various fields related to geothermal energy utilization, ranging from simulation of engineering systems to prediction of geophysical processes. A larger number of different computer models that deal with geothermal energy systems have been developed during the last decades. The scope of these models ranges from: the calculation of the heat transfer inside a borehole or the prediction of heat transport in the ground to economical optimization of GSHP (Schmidt and Hellström, 2005).

From this large availability of numerical codes, those which deal with the following two features are worth to mention on this work: a) simulations of BHEs (close systems) or/and heat extraction/injection wells (open systems) and, b) heat conduction and convection in porous media. For the first, the code must be able to represents the pipe geometry of the GSHP systems at some extent. It also should allow the user to include fundamental heat input parameters and heat extraction or/and injection rates. For the second, it should be capable of considering heat conduction and convection in the media, as for instance heat transport in confined or unconfined aquifers. To classify the programs that fulfill these requirements is a time consuming and complex task. However, some important features can work as guidelines to catalogue them such as applied numerical method, coupling of processes, self calculation of the flow field and availability of the code (commercial code or free source).

In Table 1, currently used numerical codes for heat transport simulations are listed. All these codes have in common that they consider the flow field and therefore, the effects of the groundwater flow in the GSHP system performance. Some of them as THOUGH2, HS2D/3D, SHEMAT and FEFLOW are widely used for characterization of geothermal systems (shallow and deep systems). In the following paragraphs a brief description of these codes and some of the most important features are mentioned.

AST (Aquifer storage balance)/TWOW (cited in Schmidt and Hellström, 2005): This code concerns about the heat balance of a heat extraction well (open systems). It calculates the temperature of the extracted water and the temperature in the aquifer and in the surrounding layers. The flow field must be simulated previously with a groundwater modelling code. The

code TWOW, is an extension for two wells, usually one as extraction well and another as injection well.

Table 1. Numerical codes suitable for heat transport simulations of shallow geothermal systems considering groundwater (gw) flow.

Code name	Numerical method	Calculation of flow field	Coupling of processes	Availability	Comments
AST/TWOW	FD	no	gw flow and heat transport	Private	
COMSOL	FE	yes	gw flow, heat and mass transport, mass transfer, etc	Commercial	Multi-physics = many processes can be coupled
CONFLOW	Particle tracking	yes	gw flow and heat transport	Private	
FEFLOW	FE	yes	gw flow, heat and solute transport	Commercial	
FRACture	FE	yes	gw flow, heat transport	Private	Usually use for Hot Dry Rock assessments
GEOSYS/ ROCKFLOW	FE	yes	gw flow, solute and heat transport	Private	
HST2D/3D	FD	yes	gw flow, heat and solute transport	Commercial	Powerful software and widely used
SEAWAT	FD	no	gw flow and solute transport	Free code	USGS software
SHEMAT	FD	yes	gw flow, heat and solute transport	Commercial	Suitable for geosciences applications
THETA	FD	yes	heat and solute transport	Private	
TOUGH2	FD	yes	gw, water, vapour, non-condensable gas, and heat transport	Commercial	One of the most used code in geothermal energy technologies
TRADIKON 3D	FD	yes	gw flow and heat transport	Free code	

gw= groundwater; FD: Finite Differences method; FE: Finite Elements method

COMSOL (Holzbecher and Kohfahl, 2008): It is a mathematical software tool for multiphysics modelling. It allows coupled simulation of several physical processes represented by PDEs. The user has the choice to select types or to manipulate several general forms of PDEs. For heat transport simulation, it has a particular module "Heat Transfer Module". In this module options for heat conduction and/or convection can be selected

CONFLOW (cited in Schmidt and Hellström, 2005): This code simulates the thermal front in an aquifer without considering heat diffusion and thermal dispersion. It shows graphically on screen, the groundwater flow patterns including isobars and thermal fronts.

FEFLOW (Diersch, 2002): It is a sophisticated software package for modelling fluid flow and transport of dissolved constituents and/or heat transport processes in the subsurface (saturated or unsaturated conditions). It includes interactive graphics, a GIS interface, data regionalization, visualization tools and a mesh generator. It scope of application ranges from simple local-scale to complex large-scale simulations.

FRACTure (Kohl and Hopkirk, 1995): It was developed with the specific aim of studying coupled processes in geosciences, particularly those relevant to the long term behaviour of Hot Dry Rock (HDR, deep geothermal energy). Due to the mathematical treatment of the involved processes in the simulation (fluid flow and heat transport), the code can also be applied for shallow geothermal systems. It is programmed in FORTRAN 77.

GEOSYS/ROCKFLOW V3.0 (Kolditz et al., 2001): It is a finite element code for simulating flow, heat and solute transport in porous and fractured media. It includes modules for deformation processes, multi-phases flow, gas flow and, thermal, hydraulics and mechanical coupled processes.

HST2D/3D (Kipp, 1986): It is a heat and solute transport simulation package, originally developed by the USGS and now owned by the IF Technology (The Netherlands). HST2D/3D is a powerful code and consists of four independent programs: an input processor, a simulator, an output processor and an additional utility program. The processes are coupled trough the interstitial pore velocity, the dependence of the fluid density on pressure, temperature, solute-mass fraction, and the dependence of the fluid viscosity on temperature and solute-mass fraction.

SEAWAT (Langevin et al., 2007): It is a coupled version of MODFLOW/MT3DMS designed to simulate three-dimensional, variable density, saturated groundwater flow. The code allows for coupled solute, heat and groundwater flow simulations and it includes the effect of fluid viscosity variations. Although, it is not explicitly designed for heat transport simulation, temperature can be simulated as one of the species by entering the appropriate transport coefficients (analogous approach used in this thesis).

SHEMAT (Clauser, 2003): It is a code for the simulation of stationary and transient processes in geothermal reservoirs in two and three dimensions. It is based on an earlier version (SHEMAT 4.0) for flow and heat transport (Clauser, 1988). It calculates fluid flow, heat and

mass transport as coupled or independent processes in porous media. It also includes a chemical reaction module.

THETA (Kangas and Lund, 1995): This code simulates 3D coupled flow, heat and solute transport in porous media and, it also evaluates the aquifer thermal energy storage.

TOUGH2 (Pruess et al., 1996): It is a general-purpose numerical simulation program for multi-dimensional fluid and heat flows of multiphase, multi-component fluid mixtures in porous and fractured media. Main application areas are in geothermal reservoir engineering, nuclear waste isolation studies, environmental assessment and remediation, and flow and transport in variably saturated media and aquifers. The simulation capabilities of this code are quite diverse and sophisticated, a module for three-phase, three-component, non-isothermal flow of water, air, and a volatile organic compound (VOC) and, a module for strongly coupled flow and transport in 2D systems with variable salinity and hydrodynamic dispersion, just to mention two of them. It is written in FORTRAN77.

TRADIKON-3D (Brehm, 1989): This code enables the simulation of transient mass and heat transfer in saturated heterogeneous porous media and it was specifically developed to get a better impression of the heat transfer process in the surrounding of vertical BHEs. The model allows groundwater flow simulations through an anisotropic porous medium penetrated by multiple wells or boreholes.

As can be noticed in the above description, most of the numerical codes used for heat transport simulation use the finite differences numerical method. In the next section, the finite difference method and its types are briefly explained.

2.2 Finite differences numerical method

In the finite differences method (FDM) time and space are subdivided (discretized). The considered area is first discretized in right-angles, even intervals producing a grid composed by cells. In the intersection of the grid lines (mesh centred method) or in the node of each cell (block centred method) the derivatives of the PDE to be solved are replaced with difference quotients. So each derivative is approximated by a difference quotient. The derivative equation will thus be transformed into a difference equation. Thereby one gets an equation system than can be solve by direct or iterative methods. Missing equations are supplemented with boundary and initial conditions.

The solutions obtained from the equation system are approximated solutions of the PDEs. The accuracy of these solutions depends on the grid size, grid distances and time discretization.

The FDM can be:

- Implicit method: The PDE can be solved indirectly by solving a system of simultaneous linear equations. Convergence is always assured.

- Explicit method: The PDE can be solved directly using the appropriated boundary conditions and proceeding backward in time trough small intervals until find the optimal path to every time interval. Convergence is assured for specifics size of increments in time and space.

2.3 Implementation of MT3DMS for heat transport simulations

2.3.1 Governing equations

The PDE for solute transport in transient groundwater flow systems solved by MT3DMS is written as follows (Zheng and Wang, 1999):

$$\left[1 + \frac{\rho_b K_d}{n}\right] n \frac{\partial C^k}{\partial t} = div\left(n(D_m + \alpha_s v_a)grad C^k\right) - div(v_a n C^k) + q_{ss} C_{ss} - \lambda n C^k \quad (1)$$

where:

C^k: dissolved mass concentration	[kg m^{-3}]
D_m: molecular diffusion coefficient	[m^{2}s^{-1}]
n: total porosity	[-]
α_s: solute dispersivity coefficient	[m]
v_a: seepage velocity	[m s^{-1}]
q_{ss}: volumetric flow rate per unit volume of aquifer representing sources and sinks	[m^{3}s^{-1}m^{-3}]
C_{ss}: concentration of the sources or sinks	[kg m^{-3}]
λ: Reaction rate	[s^{-1}]
ρ_b: bulk density	[kg m^{-3}]
K_d: Distribution coefficient	[m^{-3} kg]

The term of the left hand side is the transient term, which is multiplied by the retardation factor R. This dimensionless factor represents the ratio between the total solute concentration and the mobile solute concentration given by the distribution of the contaminant in the fluid and solid phase.

$$R = 1 + \frac{\rho_b K_d}{\theta} \qquad\qquad [-] \qquad\qquad (2)$$

The first term in the right hand side is the hydrodynamic dispersion term, including pure molecular diffusion (D_m) and mechanical dispersion ($\alpha_s v_a$). The second term represents the advection process and the third and fourth terms represent the source and sinks, and chemical reaction decay term respectively.

Now, the heat transport equation is discussed. This equation can be characterized by the principle of heat conservation, including conduction and convection (Marsily, 1986):

$$n\rho_w C_w \frac{\partial T}{\partial t} + (1-n)\rho_s C_s \frac{\partial T_s}{\partial t} = div\left((k_{Tm} + n\rho_w C_w \alpha_h v_a)gradT\right) - div(n\rho_w C_w v_a T) + q_h \quad (3)$$

where:

ρ_w: density of water	[kg m^{-3}]
C_w: specific heat of water	[W s kg^{-1}K^{-1}]
ρ_s: density of the solid	[kg m^{-3}]
C_s: Specific heat capacity of the solid	[W s kg^{-1}K^{-1}]
T: Temperature of the water	[K]
T_s: Temperature of the solid	[K]
k_{Tm}: Bulk thermal conductivity	[W m^{-1}K^{-1}]
α_h: Heat dispersivity coefficient	[m]
q_h: Heat injection/extraction	[W m^{-3}]

Assuming that the temperature of water and soil are the same, the term from the left hand side of the heat transport equation can be expressed as follows:

$$n\rho_w C_w \frac{\partial T}{\partial t} + (1-n)\rho_s C_s \frac{\partial T_s}{\partial t} = \rho_m C_m \frac{\partial T}{\partial t} \qquad\qquad (4)$$

thus equation (4) is simplified to:

$$\rho_m C_m \frac{\partial T}{\partial t} = div\left((k_{Tm} + n\rho_w C_w \alpha_h v_a)gradT\right) - div(n\rho_w C_w v_a T) + q_h \qquad (5)$$

where $\rho_m C_m$ is the volumetric heat capacity of the porous medium, expressed by:

$$\rho_m C_m = n\rho_w C_w + (1-n)\rho_s C_s = n\rho_w C_w + \rho_b C_s \qquad\qquad (6)$$

ρ_m: density of the porous medium	[kg m^{-3}]
C_m: specific heat of the porous medium	[W s kg^{-1}K^{-1}]

Including heat exchange with the surface where the constant of proportionality depends on the conductivity of the medium, aquifer thickness and water table depth (Mytnyk, 1978 cited in Čermák, 1985):

$$\frac{\lambda_1}{HF}\Delta T' = \text{heat exchange with the surface} \qquad (7)$$

where:

λ_1: heat conductivity of the unsaturated soil $\qquad$ [W m^{-1}K^{-1}]
H: thickness of the aquifer $\qquad$ [m]
F: depth of the water table $\qquad$ [m]
$\Delta T' = T - T_{surface}$ $\qquad$ [K]

Using this term and rearranging equation (5) we obtain:

$$\left(\frac{\rho_m C_m}{n\rho_w C_w}\right)n\frac{\partial T}{\partial t} = div\left(n\left(\frac{k_{T\,m}}{n\rho_w C_w}+\alpha_h v_a\right)gradT\right) - div(nv_a T) + \frac{q_h}{\rho_w C_w} - \frac{\lambda_1}{\rho_w C_w HF}\Delta T' \qquad (8)$$

where $\quad D = \dfrac{k_T}{n\rho_w C_w}+\alpha_h v_a \quad$ is the heat dispersion coefficient $\qquad$ (9)

and $\quad R = \dfrac{\rho_m C_m}{n\rho_w C_w} \quad$ is the retardation factor $\qquad$ (10)

2.3.2 Conforming coefficients and its inclusion in MT3DMS

As mentioned above, solute and heat transport processes in groundwater can be described with similar differential equations. In order to relate equations (1) and (9), the coefficients can be compared as follows:

Solute transport equation:

$$\left[1+\frac{\rho_b K_d}{n}\right]n\frac{\partial C}{\partial t} = div\left(n\left(D_m+\alpha_s v_a\right)gradC\right) - div(v_a nC) + q_{ss}C_{ss} - \lambda nC$$

| Solute sorption | Solute diffusion and | Advection | Sources and sinks | Chemical reaction |

Heat transport equation:

$$\left(\frac{\rho_m C_m}{n\rho_w C_w}\right)n\frac{\partial T}{\partial t} = div\left(n\left(\frac{k_{T\,m}}{n\rho_w C_w}+\alpha_h v_a\right)gradT\right) - div(nv_a T) + \frac{q_h}{\rho_w C_w} - \frac{\lambda_1}{\rho_w C_w HF}\Delta T'$$

| Thermal equilibrium | Solute diffusion and dispersion | Convection | Heat injection-extraction | Heat exchange |

Next, each term and its inclusion in MT3DMS will be described in detail:

- Retardation factor and distribution coefficient (Thermal equilibrium)

The retardation factor and the distribution coefficient, represented in the solute transport equation as solute sorption, can be equivalently expressed in the heat transport equation as a thermal equilibrium, representing the heat exchange between the solid and the water.

In the first term from the heat transport equation, the retardation factor for heat given as the ratio between the volumetric heat capacity of the porous medium (total phase) and the volumetric heat capacity of the water (mobile phase) is identified:

$$R = \frac{\rho_m C_m}{n \rho_w C_w} \qquad\qquad [-] \qquad\qquad (11)$$

Making equal the retardation factors from solute and heat transport, the distribution coefficient expressed as a function of heat parameters is as follows:

$$1 + \frac{\rho_b K_d}{\theta} = \frac{\rho_m C_m}{n \rho_w C_w} \quad \rightarrow \quad K_d = \frac{\rho_m C_m}{(\rho_w C_w) \rho_b} - \frac{n}{\rho_b}$$

$$K_d = \frac{C_s}{(\rho_w C_w)} \qquad\qquad [\text{m}^3\text{kg}^{-1}] \qquad\qquad (12)$$

That means that the temperature exchange rate between the solid and the fluid will be constant through the temperature range.

> The new distribution coefficient for heat transport is implemented in MT3DMS in the *Chemical Reaction Package* and the type of sorption must be set to *linear isotherm (ISOTHM=1)*.

- Diffusion and dispersion coefficients

In the diffusion and dispersion term of the partial differential equation for solute transport (eq. 1), two parts are identified:

$$(D_m + \alpha_s v_a)$$

A pure molecular diffusion term (D_m) that represents a process driven only by the concentration gradient. It is equivalent in the heat transport equation to the thermal diffusivity which is, in this case, driven by the temperature gradient:

$$D_m = \frac{k_{Tm}}{n\rho_w C_w} \qquad [\text{m}^2\text{s}^{-1}] \qquad (13)$$

The second term, $\alpha_s v_a$, which is hydrodynamic dispersion, which is a process driven by the differences in flow velocities. For the implementation in MT3DMS the solute dispersivity coefficient is simple replace by the heat dispersivity coefficient.

$$\alpha_s = \alpha_h \qquad [\text{m}] \qquad (14)$$

The new diffusion coefficient and the dispersivity coefficient are implemented in the *Dispersion Package*.

- Sources and Sinks

The source an sink term in the solute transport equation represents the mass entering or leaving the domain through source and sinks. In the heat transport equation, this source and sink terms indicate energy input or extraction.

$$q_{ss}C_{ss} = \frac{q_h}{\rho_w C_w} \qquad [\text{K s}^{-1}] \qquad (15)$$

To be consistent with the dimensions relating the contaminant and heat transport, the dimension Kelvin [K] is equivalent to the concentration [kg m^{-3}]. That means that: [Ks^{-1}] = [kg m^{-3}s^{-1}], which is a mass load per unit volume of aquifer.

The new source and sink term for heat transport is implemented in MT3DMS in the *Sink & Source Mixing Package* and the type of source must be set to a *mass-loading source (ITYPE0=15)*.

- Heat exchange with the surface

Based on equation (7), for quantifying the heat exchange with the surface over the unsaturated zone, the following conforming coefficient for the reaction rate is obtained:

$$\lambda = \frac{\lambda_1}{\rho_w C_w HF} \qquad\qquad [s^{-1}] \qquad\qquad (16)$$

> The new reaction term for heat transport is implemented in MT3DMS in the *Reaction Package* and in a three-dimensional heat transport model has to be assigned only at the top layer.

It must be also point out that this term was not included in the verification of MT3DMS, but it is an important task for future work.

2.4 Analytical solutions

In this section, the analytical solutions to be used for the verification of MT3DMS for heat transport simulation are presented. A comprehensive description of these analytical solutions can be found in the thesis "Verification of MT3DMS as a heat transport code using analytical solutions" (Molina, 2008).

In Table 2, the analytical solutions to be used for the verification of the MT3DMS are listed. Later, each of them is briefly described.

Table 2. List of analytical solutions.

Type of problem	Analytical solution	Observation
Only conduction (without flow velocity)	Line source model, continuous source	2D, transient conditions, closed systems
Convection	Point model, continuous source	3D, steady state, closed systems
Convection	Planar source, continuous source	3D, transient conditions, closed systems

- Line source model (Carslaw and Jeager, 1959)

The analytical solution for transient conditions, continuous source, close system and no flow velocity is as follows for 2-dimensions and line source (Figure 2).

$$T(r,t) = \frac{F_o}{4\pi k_{Tm}} Ei\left[-\frac{r^2}{4(k_{Tm}/\rho_m C_m)t} \right] \qquad\qquad (17)$$
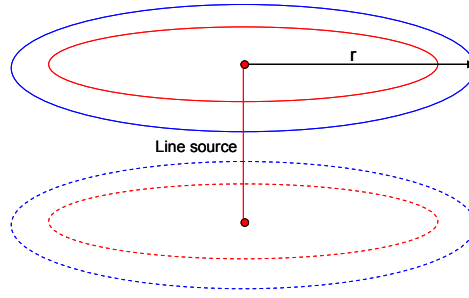
Figure 2. Heat plume spreading for the analytical solution with line source and no flow velocity.

- Point source, 3D (analogous to Fried et al. 1979)

The analytical solution analogous to Fried et al. (1979) for steady state, continuous source and closed system is as follows for 3-dimensions and point source (Figure 3):

$$T(x,y,z) = \frac{F_o'}{v_a n \ \rho_w C_w 4\pi D_{yz} \frac{x}{v_a}} \exp\left(\frac{-v_a(y^2+z^2)}{4D_{yz}x}\right) \tag{18}$$

where F_o' is the energy extraction in one point [W] and D_{yz} is the dispersion coefficient for transversal dispersivities in y and z direction (α_{hy}, α_{hz}). In this analytical solution, infinite transversal dispersion has to be considered.
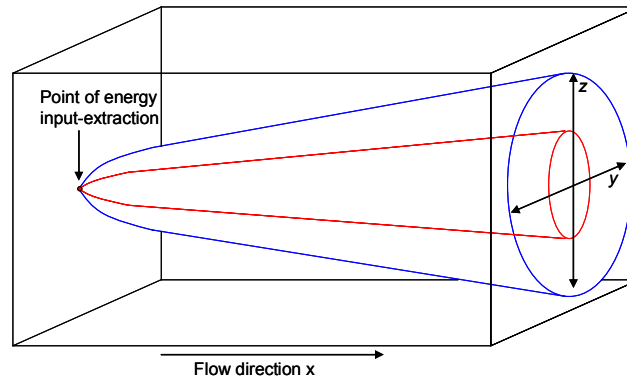
Figure 3. Heat plume spreading for the 3D analytical solution with point source.

- Planar source, 3D (analogous to Domenico and Robbins, 1985)

The analytical solution analogous to Domenico and Robbins (1985) for transient conditions, continuous and planar source, and closed system is as follows (Figure 4):

$$T(x,y,z,t) = \left(\frac{T_0}{8}\right) erfc\left[\frac{(Rx-v_a t)}{2\sqrt{D_x Rt}}\right] \left\{ erf\left[\frac{(y+Y/2)}{2\sqrt{D_y \frac{x}{v_a}}}\right] - erf\left[\frac{(y-Y/2)}{2\sqrt{D_y \frac{x}{v_a}}}\right] \right\}$$

$$\left\{ erf\left[\frac{(z+Z/2)}{2\sqrt{D_z\frac{x}{v_a}}}\right] - erf\left[\frac{(z-Z/2)}{2\sqrt{D_z\frac{x}{v_a}}}\right] \right\} \tag{19}$$

The dimensions of the source are given by Y and Z. The dispersion coefficients D_x, D_y and D_z are given by the equation (9), for dispersivities in x, y and z directions (α_{hx}, α_{hy}, α_{hz}). T_o is the initial temperature in the point of energy extraction and is given by the following equation:

$$T_0 = \frac{F}{v_a n \rho_w C_w} \tag{20}$$

where F is the energy extraction per area of the source [W m^{-2}]

For the centreline of the plume ($y = z = 0$), the equation (19) becomes:

$$T(x,t) = \left(\frac{T_0}{2}\right) erfc\left[\frac{(Rx - v_a t)}{2\sqrt{D_x Rt}}\right] erf\left[\frac{Y}{4(D_y\frac{x}{v_a})^{0,5}}\right] erf\left[\frac{Z}{4(D_z\frac{x}{v_a})^{0,5}}\right] \tag{21}$$
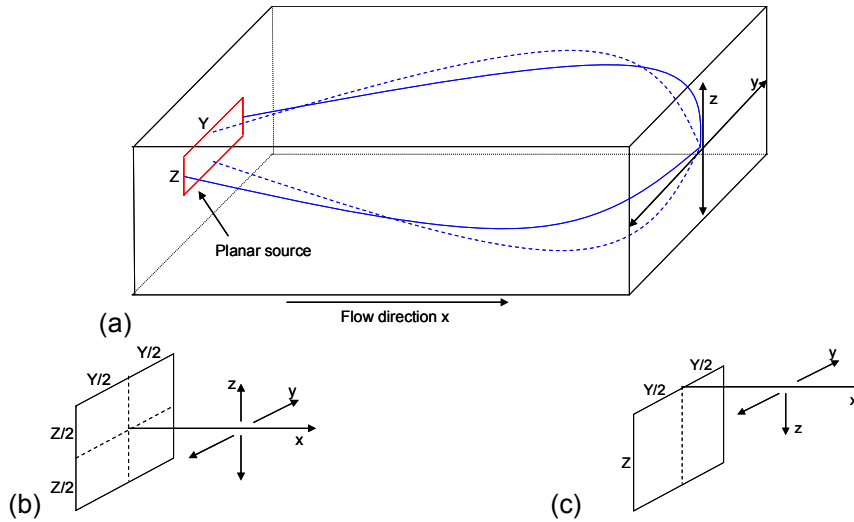
Figure 4. (a): Heat plume spreading for the analytical solution with planar source. (b): two spreading directions in *y* and *z*. (c): two spreading directions in *y* and one *z*.

For steady state conditions, the complementary error function (*erfc*) term is neglected and the ($T_0/2$) term becomes T_0:

$$T(x) = T_0 erf\left[\frac{Y}{4(D_y\frac{x}{v_a})^{0,5}}\right] erf\left[\frac{Z}{4(D_z\frac{x}{v_a})^{0,5}}\right] \tag{22}$$

3 ADOPTION OF MT3DMS FOR HEAT TRANSPORT SIMULATION

As it was stated previously, the use of MT3DMS for heat transport modelling can be performed, if the conforming coefficients of the partial differential equation are identified and exchanged. Additionally, the user must have a deep understanding of how to use the numerical code for heat simulations.

In this chapter it is showed in a step-forward fashion, how to make use of the MT3DMS capabilities for heat transport modelling. The following aspects are evaluated: first, setting up of the boundary conditions for a typical configuration of a ground source heat pump system. In this step, an assessment of the best boundary condition to be used in order to decrease boundary effect is done. Second, the choice of the advection solver according to the flow velocity field is discussed. MT3DMS offers various solvers for solving the advection term of the solute transport PDE. The appropriate selection of the type of solver is crucial as it controls, 1) the accuracy of the final results, 2) the degree of numerical dispersion and/or numerical oscillation obtained in the simulation and 3) the execution time of the simulation. Therefore, the five advection solvers included in MT3DMS for three flow velocities are compared. Third, discretization at the cell where the source/sink is located cell. Various discretization variants are compared with the analytical solution.

A unique feature of MT3DMS is the option to enter the macrodispersion coefficient in 2D or 3D arrays. Two scenarios are compared, one with the coefficient evenly defined in the whole domain and other with the coefficient partially defined. Likewise, the length of the heat plume is calculated for different values of the hydrodynamic dispersivity.

3.1 Conceptual models

Figures 5 and 6 depict conceptual 2D and 3D models to be used throughout the various analyses in this chapter. The 2D conceptual representation is a one-layer model, with a discretization of 1 m × 1 m per cell, representing a confined aquifer. The layer is 1 m thick. For the 3D case (Figure 6), a similar conceptualization is used with same properties, however several layers are used. In the 3D case, the source is always placed in the centre layer of the model. In order to consider only horizontal flow, a low vertical hydraulic conductivity between layers was used (1E-8 m/s). In this way, only lateral heat transport is considered in the analyses.
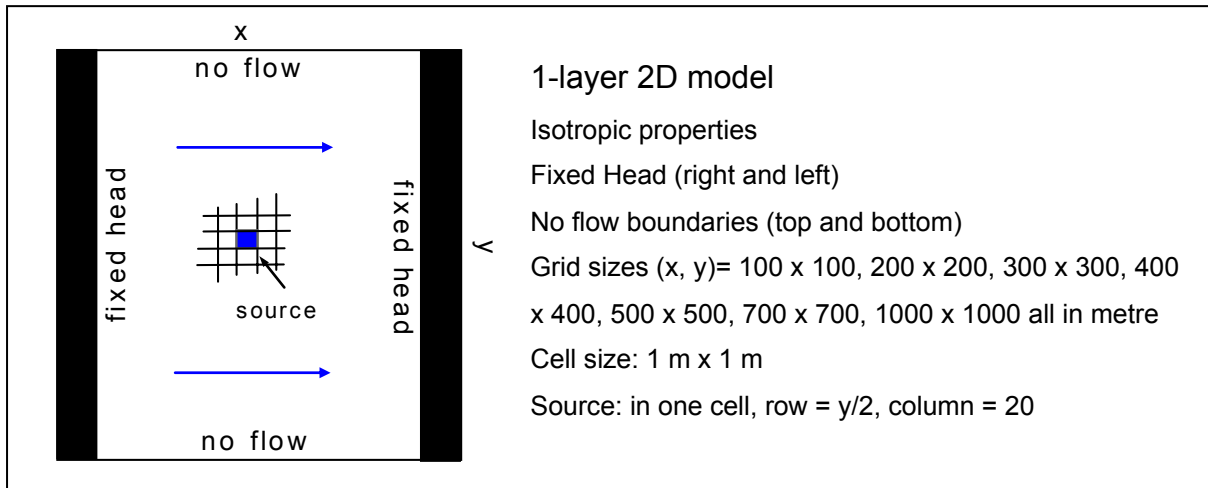
Figure 5. Conceptual model for the 2D case. Blue square and arrows represent the sink/source cell and flow direction respectively.

For either 2D or 3D cases, the source is placed in one cell and it represents a borehole heat exchanger as used in GSHP systems for heating purpose. Under this assumption, heat is extracted from the thermal reservoir, i.e. the aquifer. Since energy is extracted from the medium, the respective input value for the cell where the sink is located (source cell) must be assigned negative in the source and sink package (SSM) of MT3DMS.
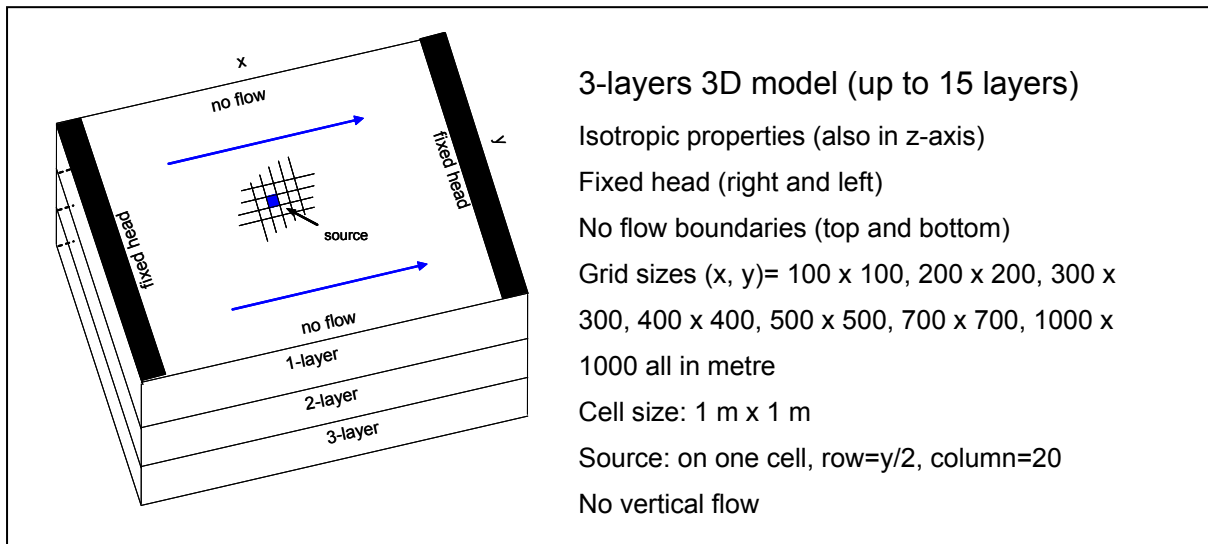
Figure 6. Conceptual model for 3D case. Three layers example. Blue square and arrows represent sink/source cell and flow direction respectively.

3.2 General methodology

This section presents common aspects in the methodology to be applied in the various evaluations described in this chapter.

Hydrogeological and heat parameters: Some input data are common for all the evaluations, as for instance: flow velocity, 3.2E-6 m/s (k = 8.0E-3 m/s, i = 4.0E-4) and energy extraction, 60 W. The first is within the range of flow velocity for sand aquifers, while the energy extraction corresponds to values of energy extraction as used in GSHPs (Clauser et al., 2003, Clauser, 2006). A list of other common parameters used for the flow model (MODFLOW) and for the heat simulation (MT3DMS) is in Table 3. In this list, names of the MT3DMS/MODFLOW packages to be used and the keyword of the respective parameters are showed.

Numerical results: The code MT3DMS has the option of locating observation points in the grid and performing lectures of the results for a given time or various times selected by the user. The application of these points is done via the basic package BTN. For both 2D and 3D models, the points are located as showed in Figure 7. In total, 200 points are activated, except for grid size of 100 m × 100 m, where only 60 points are used. After each simulation, an ASCII file with the numerical results is created. The data is processed with a routine developed in MATLAB (Anibal Pérez, personal communication), and subsequently, the results are brought into EXCEL, where tables and figures are elaborated.
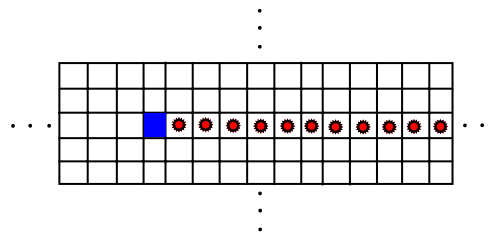
Figure 7.Sketch of the observation point's location for 2D cases (analogous for 3D cases). Blue square represents source cell. Red circles are the observation points located downgradient along the x-axis.

Analytical results: The equations for the analytical solutions to be used in the verification (eqs. 17, 18, 21 and 22), are implemented in MATLAB and EXCEL. The outputs from MATLAB are saved in ASCII files and later entered in EXCEL.

Visualization of the 2D and 3D numerical results: For visualization of the numerical results obtained with MT3DMS, the software MODEL VIEWER by Hsieh and Winston (2002) is used. Heat plume visualizations for two scenarios are showed in the verification chapter.

Table 3. Input parameters for MODFLOW and MT3DMS

MODFLOW				
Parameter	**Value**	**Units**	**Package**	**Keyword**
$\Delta x = \Delta y$	1.00	m	DIS	DELR, DELC
Gradient (i)	4.00E-4	-	FHB	-
Darcy´s velocity (v)	3.20E-6	m s^{-1}	-	-
Seepage velocity (v_a)	1.23E-5	m s^{-1}	-	-
h_o (initial head)	2	m	FHB/BAS	-
h_i (head at the first column)	2	m	FHB	
h_f (head at the last column	1.84	m	FHB	
Tansmissivity (T)	8.00E-3	m s^{-1}	BCF	TRAN
MT3DMS				
Parameter	**Value**	**Units**	**Package**	**Keyword**
Effective porosity (n_e)	0.26	-	BTN	PRSITY
Specific heat capacity soil solid (c)	880	-	-	-
Volumetric heat capacity soil (ρc_s)	2.33E+6	J m^{-3}K^{-1}	-	-
Volumetric heat capacity water (ρc_w)	4.19E+6	J m^{-3}K^{-1}	-	-
Volumetric heat capacity porous medium (ρc_m)	2.81E+6	J m^{-3}K^{-1}	-	-
Thermal conductivity (λ)	2	W m^{-1}K^{-1}	-	-
Initial Temperature (T_o)	285.15	K	BTN	SCONC
Stress period	6912E+4	s	BTN	PERLEN
Longitudinal dispersivity (α_L)	5	m	DSP	AL
Ratio of horizontal transverse dispersivity (α_{TH})	0.01	-	DSP	TRPT
Ratio of vertical transverse dispersivity (α_{TV})	0.01	-	DSP	TRPV
Thermal diffusivity	1.84E-6	m^{2}s^{-1}	DSP	DMCOEF
Bulk density	1961.0	g cm^{-3}	RCT	RHOB
Distribution coefficient K_d	2.10E-4	-	RCT	SP1
Energy extraction	60	W	SSM	CSS

3.3 Model boundary conditions

As for mass transport modelling, two boundary conditions have to be defined for heat transport simulation. One for the flow model (MODFLOW) and another for the heat transport model (MT3DMS). For the flow model, Dirichlet boundary conditions are used. It means that the hydraulic heads remain spatially and temporarily constant throughout the simulations and they are only assigned at the beginning of the simulation (time zero). The heads are allocated at the first column and at the last column and their values will depend on the gradient to be

used in the model. For the heat model constant temperature (285.15 K) is assigned in the first column, which is the initial temperature of the entire model.

As for solute transport modelling using MT3DMS, for heat transport simulations the definition of the grid size is also a crucial step in order to diminish boundary effects that can influence the results. The distance between the source cell and the borders of the model must be large enough to avoid influences of the limits of the simulation domain. Moreover, the configuration of the model must provide an extended region downgradient, in which the plume can develop during the simulation. For the latter, the user must be aware that the larger the grid size, the larger the running time of the simulation. If this condition is not carefully considered, for complex models the hardware requirements would increase considerably. For these reasons, it becomes important to determine the minimum size of the grid for which accurate results can be achieved.

3.3.1 Method

To analyse the boundary effects, 6 different grid sizes are used: 100 m $\times$ 100 m, 200 m $\times$ 200 m, 300 m $\times$ 300 m, 400 m $\times$ 400 m, 500 m $\times$ 500 m, 700 m $\times$ 700 m and 1000 m $\times$ 1000 m. For all cases the cell size is 1 m $\times$ 1 m.

The boundary conditions for the flow model are set up using the package "Flow and head boundary package (FHB)". This package permits to assign fixed hydraulic heads for a specific column at a determined time. Since the simulation is steady state, the heads are assigned only once in the beginning of the simulation, i.e. time equal to zero. For the heat transport simulation, the condition at the first column is set to constant temperature (285.15 K) through the number -1 (constant cell), and the rest of the cell are set to active cells through the number 1. The latter is necessary for the case that the plume reaches the downgradient boundary. Nevertheless, only the grid size is of particular interest in this section. For 3D case, the boundary effects in the z-axis are also analyzed for scenarios with several layers (3, 5, 7, 9, 11, 13, 15 layers).

The 2D numerical results are compared with the following analytical solution: point source, with flow velocity (eq. 18), and for the 3D results: planar source, with velocity (eq. 22), both for steady state conditions.

3.3.2 Results

2D CASE

The curves of the MT3DMS results and the analytical solution up to 60 meters, for each grid size are depicted in Figure 8. For the smallest grid size (100 m × 100 m), the curve of the numerical results does not match at all with the analytical solution curve. This is due to the influence of the boundaries in the numerical results. For grid sizes ranging from 200 m × 200 m to 500 m × 500 m, the match between the curves is good at distance from the source larger than 2 m. The difference of about 0.25 K, near the source, is due to other effect that that will be investigated in the last section of this chapter. For grid sizes larger than 500 m × 500 m, the curves of the simulated results get slightly further away from the analytical solution, for instance, for 700x700 m, the temperature difference reaches up to 0.3 K. It is possible that for these large grid sizes, a regional component is being included in the model, causing a smoothing out of the effect of the energy extraction cell on the media. This situation leads to a deviation of the numerical results from the analytical solution.
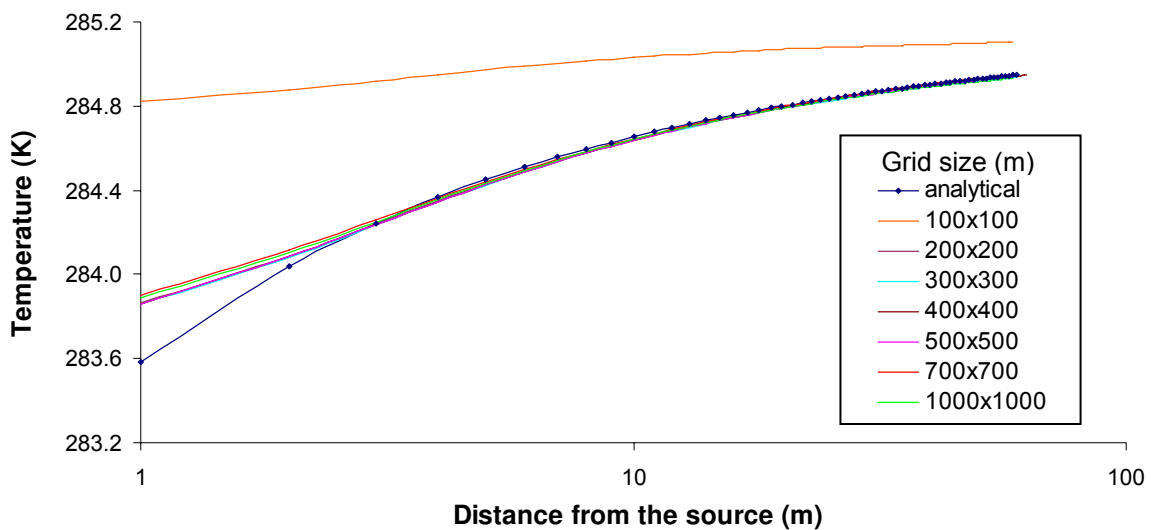
Figure 8. Comparison of the 2D numerical results with the analytical solution for various grid dimensions in logarithmic scale.

It can be concluded that the best grid size for further work, with the current input parameters and configuration, is between 200 m × 200 m and 500 m × 500 m. Nevertheless, higher area size can be used because the temperature differences between numerical and analytical results for these cases are low.

3D CASE

Figure 9 depicts the comparisons of the 3D numerical results with the analytical results. For the smallest area size (100 m × 100 m), the numerical and analytical curves considerably differ from each other, as well as for 1000 m × 1000 m. As for the 2D case, boundary effects occur for the smallest grid size. For the highest grid size, the difference can be addressed to the inclusion of a regional component as mentioned above. In contrast to 2D cases, the regional component in the 3D case causes a larger influence on the numerical results, leading to a deviation for the numerical results for 1000 m × 1000 m. The best approximations are found for grid size ranging from 200 m × 200 m to 700 × 700 m. Within this range, temperature differences between numerical and analytical results tend to decrease as the distance from the source gets larger, from 0.311 to 0.318 K at 1 m from the source down to 0.026 to 0.029 K, at 60 m from the source. As for the 2D case, the observed difference is due to a phenomenon that is discussed in the last section of this chapter. From these results it can be concluded that a grid size of 200x200 m is the minimum acceptable for heat modelling with similar configuration. This grid size guarantees that any boundary effect will affect the numerical results and it also reduced considerably the execution time.
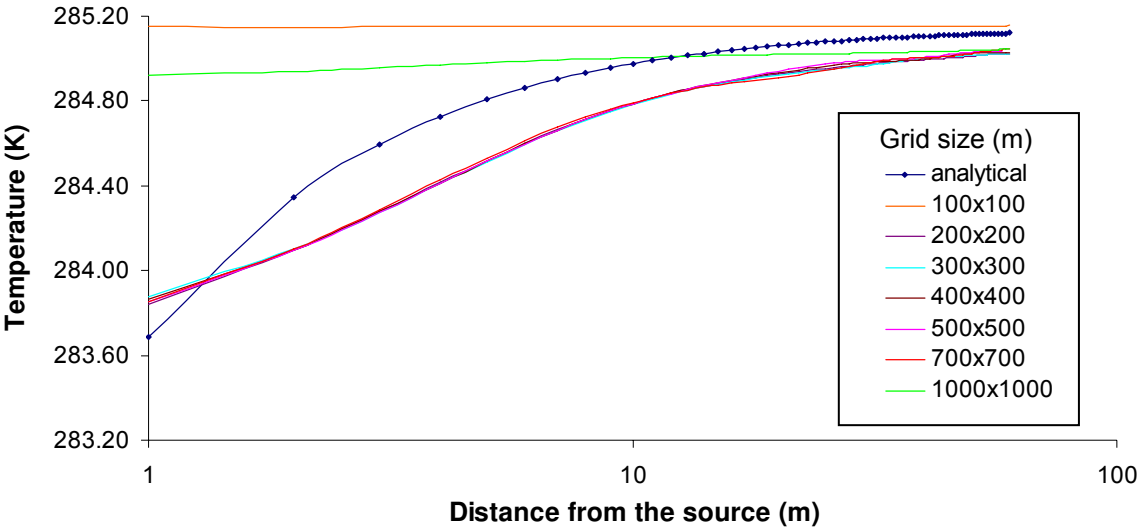
 Figure 9. Comparison of the 3D numerical results with the analytical solution for various grid dimensions.

To evaluate the boundary effect in the z-axis, a grid size of 400 m × 400 m is used and simulations are ran for various number of layers, starting with 3 layers up to 15 layers. Figure 10 shows the MT3DMS results compared with the analytical solution. It can be observed that from 7 layers on, there is not a significant difference between the simulated results. Only for the first two cases (3 and 5 layers), numerical curves show a larger deviation from the analytical one. Comparing Figure 9 and 10, the match between numerical and analytical

results improves, when more layers are include into the model. Then, boundary effects on the z-axis can be effectively reduced if more layers are used in the model. The fit is particularly good for distance from the source larger than 20 m. Based on these results, for heat modelling of 3D cases, a minimum of 7 layers are recommended. With this minimum number of layers, boundary effect in the z-axis is diminished for the current setup. The remaining difference observed in Figure 9 and 10 are also partly due to other effect that is studied in the last section of the present chapter.
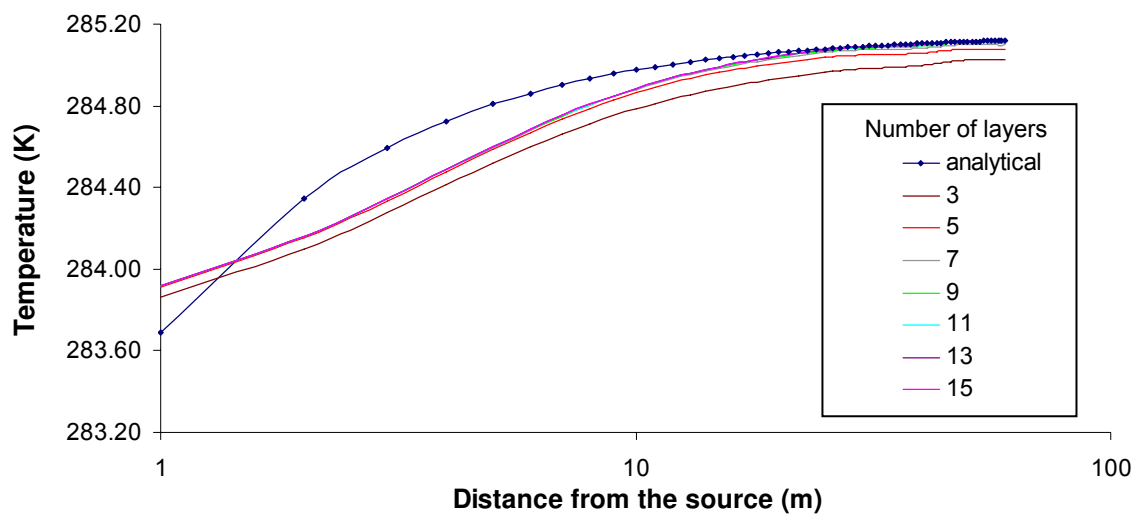
Figure 10. Comparison of 3D numerical results with the analytical solution for various numbers of layers.

3.4 Advective transport solution options

MT3DMS is unique software because it has five different solver solutions for the advection term of the mass transport partial differential equation. Each of these solution options has its advantages and disadvantages depending on the type of problem to be modelled and the goals to be reached by the modellers. Some of these methods aim to obtain more accurate simulated results with lower or any numerical dispersions and numerical oscillation, as the mixed eulerian-lagrangian methods (method of characteristics, modified method of characteristics and hybrid method of characteristics), and the third order TVD (eulerian method). On the other hand, eulerian methods (standard finite-difference method, implicit and explicit), are faster and they need less computer requirement but the accuracy of the simulated result can be lower for some situation as for instance advection dominated problems. Therefore a relation efficiency-accuracy is raised when using MT3DMS. The purpose of this chapter is to show, which solver is more suitable for a specific flow field.

3.4.1 Method

Five solvers are applied for simulating heat transport in a 2D model for three different flow velocities as showed in Table 4. The grid size is 400 m × 400 m and the hydrogeological parameters are the same as for the previous analyses. The courant number for all cases is 1 and the simulation time is 4000 days, this time length guaranties steady state conditions. The total running times of the simulations are recorded for each advection solver.

Table 4. Tested advection solution options.

Seepage velocity (m s^{-1}), gradient, PE	Advection solver	Convergence error criterion	Observations
1.85E-6, i = 6.0E-5, Pe =1 1.23E-5, i = 4.0E-4, Pe=7 3.69E-5, i = 1.2E-3, Pe =20	Standard finite difference	1.0E-10	Upgradient weighting
	Method of characteristics	1.0E-10	
	Modified method of characteristics	1.0E-9	
	Hybrid method of characteristics	1.0E-9	
	Third order TVD (ULTIMATE)	1.0E-6	

3.4.2 Results

In Table 5, execution time of the simulations for each hydraulic gradient and each solver are listed. The „fastest" advection solver is the finite difference method with 1.3 min and 4 min for gradients i = 6.0E-5 and i = 4.0E-4, respectively. For the gradient i = 1.2E-3, this solver does not provide any results. The running times for the method of characteristic and its variants (modified and hybrid) are quite equal and they are approximately twice than those for the finite difference. For instance, for gradient i = 4.0E-4 the execution time for MOC was 10 min, while for finite differences was only 4 min. The third order TVD (ULTIMATE) is the "slowest" advection solver used for all gradients.

Table 5. Running time for each advection solver method.

	TIME (min)				
gradient i	HMOC	FINITE DIFF.	MOC	MMOC	ULTIMATE
1.2E-3	27.3	n/a	27.4	26.8	34.1
4.0E-4	9.9	4.0	10.0	9.7	13.0
6.0E-5	1.8	1.3	1.8	1.8	2.5

The comparison of the numerical results and the analytical solution for all cases is depicted in Figure 11. For i = 6.0E-5 (Pe =1), the best match is found for the modified and hybrid method of characteristics. On the other hand, for sharp front problems (Pe = 7 and Pe = 20), all solvers show a good fit between numerical and analytical solutions, except for the finite difference solver which was not able to converge for Pe = 20. Nevertheless, when the solvers are qualitatively compared, the third order TVD (ULTIMATE) method shows the lowest temperature difference between numerical and analytical results.
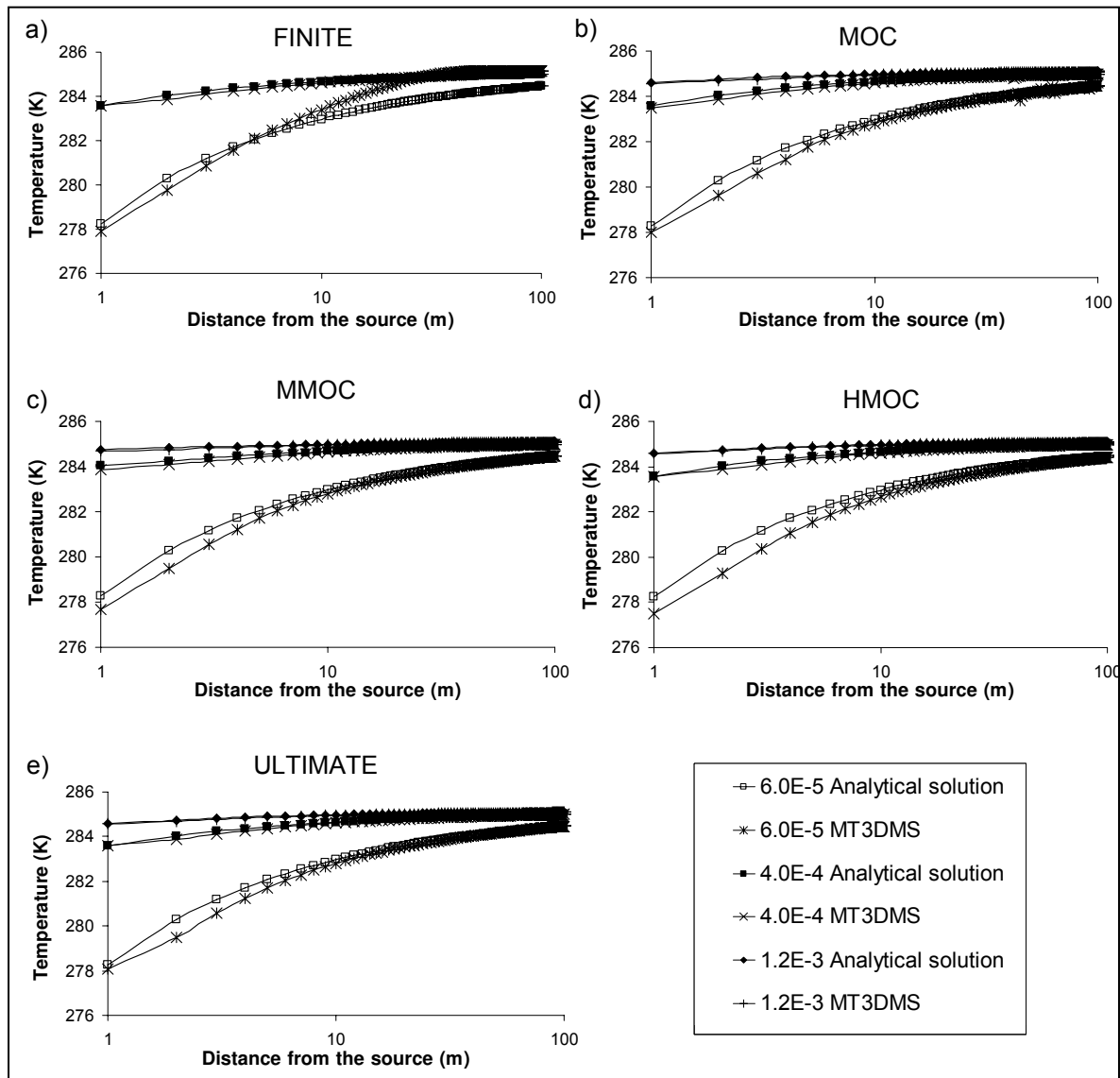
Figure 11. Comparison between numerical and analytical results for three gradients applying the five advection solver methods included in MT3DMS. a)Finite difference, b)Method of characteristics (MOC), c)Modified method of characteristics (MMOC), d)Hybrid method of characteristics (HMOC) and e)Third order TVD (ULTIMATE).

From these results and based on the scope of the present work, the ULTIMATE scheme will be used for the next analyses and for the verification chapter. Although the ULTIMATE

method requires more time and more computer capabilities, this solver gives more accurate results, an important aspect for the numerical verification of the code.

3.5 Discretization at the heat extraction cell

As it was explained in the theoretical background chapter, the analytical solutions are mathematical representation of: a line source (2D), point and planar source (3D). In these representations, an infinitesimal point or line and an infinitesimal plane in the x-axis are assumed. In order to analyse the capabilities of MT3DMS for heat transport modelling under this mathematical assumptions, simulations with a discretized cell where the source is located are necessary, now on, we will refer to this cell as source cell. The source cell is subdivided down to the dimensions of a borehole heat exchanger. Generally, the diameter of a BHE is 0.15 meter (15 cm).

3.5.1 Method

For the analyses, six simulations are performed for models with various size of the source cell. The cell size is decreased systematically as follow: 10 m × 10 m, 5 m × 5 m, 3 m × 3 m, 1 m × 1 m, 0.5 m × 0.5 m and 0.15 m × 0.15 m. It is important to point out that the discretization at the source cell must be also applied in the flow model (MODFLOW) before the use of MT3DMS. Based on the finding in previous sections, this test is performed with a grid size of 400 m × 400 m.

For the 3D case, the discretization of the source cell in the z-axis is also evaluated for planar source. First, the effect of the discretization in the x,y-axes is analyzed for a constant layer thickness (1 m). Second, two cases are studied: a) energy extraction in one cell with 3 m thickness and, b) source in 3 cells with same thickness (3 layers of 1 m each). The 3D model comprises 9 layers.

3.5.2 Results

2D CASE

In Figure 12 the comparison between the numerical and analytical results for the six discretizations at the source cell are showed. As can be clearly seen, the smaller the size of the heat extraction cell, the better the fit between the curves. Indeed, the best approximation was obtained for a source cell size of 0.15 m × 0.15 m. Therefore, it has been proved that entering

geometries of a BHE is feasible with certain degree of confidence. If this tendency is constant, the match between the curves is expected to improve for smaller source cell sizes. Nevertheless, this task is out from the objective of the present work. Another aspect that should be considered is the running time of each simulation. As the size of the source cell is decreased, the execution time of the simulation increases considerably.
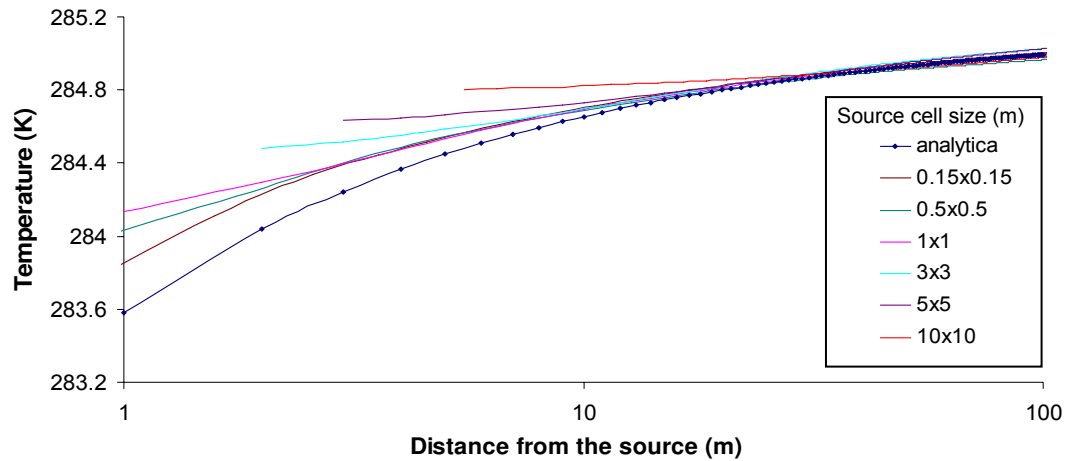
Figure 12. Comparison between the 2D numerical and analytical solution for various source discretizations.

3D CASE

Simulations for source cell sizes of 1 m × 1 m, 0.5 m × 0.5 m and 0.15 m × 0.15 m are presented. Analogously for the z-axis, numerical results for source cell size of 1 m × 1 m, 0.5 m × 0.5 m and 0.15 m × 0.15 m are showed. Figure 13 shows the comparison between the simulated results and the analytical solution. For the three dimensions in the x,y-axes, the matches between the simulated and the analytical curves are good at distances from the source larger than 10 meters, with the best being 0.15 m × 0.15 m, the same as the 2D case (Figure 13, graph c). For the latter, despite of the temperature differences near the source, the simulated curve follows the tendency of the analytical solution along the temperature profile. The other two scenarios have larger temperature differences along the profile and even they cross the analytical curve at one point.

In Figure 14 the curves for discretizations of the source cell in the z-axis are showed. As it can be seen, the numerical results for cases a) and b) are quite equal each other. Within the first 4 m distance from the source, there is still a temperature difference of about 0.4 K between numerical and analytical solutions. This dissimilarity is partly due to the upgradient effect and it is discussed in the next analysis "role of macrodispersivity"
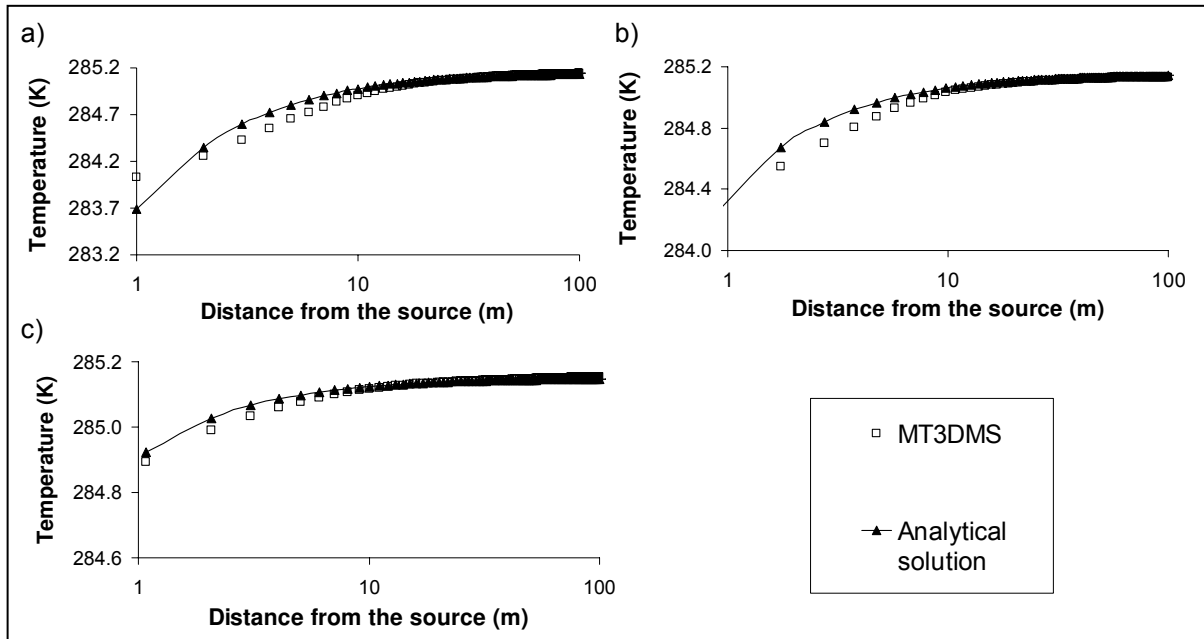
Figure 13. Comparison between 3D analytical and numerical results for various cell source discretizations (x,y-axes). Source cell sizes: a) 1 m × 1 m, b) 0.5 m × 0.5 m and c) 0.15 m × 0.15 m.

Based on the results obtained in this section, for the verification chapter we will use a source cell size of 0.15 m × 0.15 m (x,y-axes). For 3D cases, the thickness will be 3 m with the source in 3 cells, 1 m each.
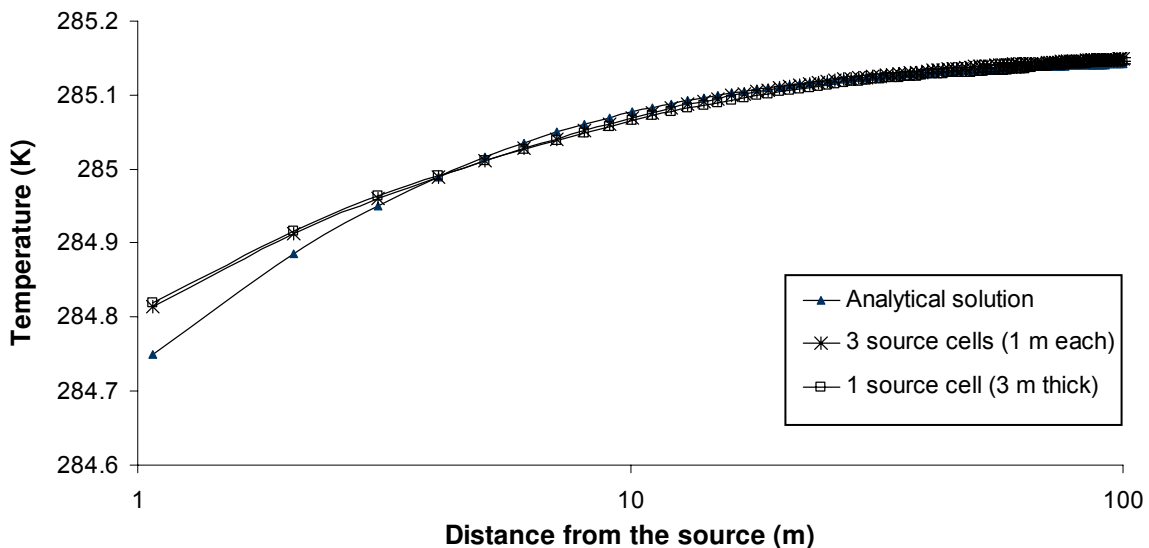
Figure 14. Comparison between analytical and numerical results for two types of source discretizations (z-axis). a) Source in three cells with 1 m thickness each, b) one source cell with 3 m thickness.

3.6 Role of macrodispersivity

An important aspect to be considered in heat transport problems is the hydrodynamic macrodispersion (Ferguson, 2007). The macrodispersion coefficient involves the thermal

difussivity (k_t) and the hydrodynamic dispersion (α_h), as described by equations (13) and (14). A comprehensive analysis of this macrodispersion coefficient for heat transport simulations is found in Molina (2008).

Throughout the previous analysis the macrodispersion coefficient has been evenly defined for all the scenarios. This configuration has caused an upgradient dissipation of the thermal energy near the source. Due to this phenomenon, a temperature difference between analytical and numerical results in this region has been also observed in the previous studies (Grathwohl, personal communication). Moreover, the analytical solutions are semi-infinite formulations; it means that they do not consider the upgradient effect in the calculations.

Due to the reasons mentioned above, a procedure must be applied that allows neglecting this upgradient effect in the numerical code. The unique capabilities of MT3DMS include the possibility of passing this effect over via the multidiffusion option (MT3DMS v5.2, supplementary guide. Zheng, 2006). This option permits to assign values of hydrodynamic dispersion (α_h), and also of thermal diffusivity (k_t) cell by cell within the model. In this section results using this option are showed. Additionally, the relation between various values of hydrodynamic dispersion and the length of the plume are also evaluated.

3.6.1 Method

For analysing the upgradient effect, a model with a uniform macrodispersion coefficient value for the entire area, is compared with a model set up applying the multidiffusion option. Using this option, the α_h and k_t values are set to zero at the columns behind the source cell. Since the extraction cell is located in column 100, the values of thermal diffusivity and hydrodynamic dispersion for columns 0 to 99 are set to zero.

To studying the relation between the hydrodynamic dispersion and the length of the heat plume, five simulations with 5 different values of hydrodynamic dispersion (α_h = 5, 4, 3, 2 and 1 m) are performed. The plume lengths for the isotherm 285.10 K for each simulation are saved. Then, the results are shown in a diagram with hydrodynamic dispersion versus length of the plume. The model configuration for this analysis is 2D, gradient i = 4E-4 and heat extraction in one cell (60 W) with discretization of 0.15 m × 0.15 m.

3.6.2 Result

Figure 15 depicts the numerical results for the models with the macrodispersion coefficient evenly and partially defined in the domain. The respective analytical results (eq. 20) are included.

The curve for the numerical result with the coefficient values evenly defined in the entire area shows a larger temperature difference when compared to the analytical solution. On the other hand, when the multi-diffusion option is used, i.e. the macrodispersivity values where assigned only for downgradient cells, the difference is smaller. This is due to the fact that heat that in the first case is dissipated upgradient is highly diminished when the multidiffusion option is used.
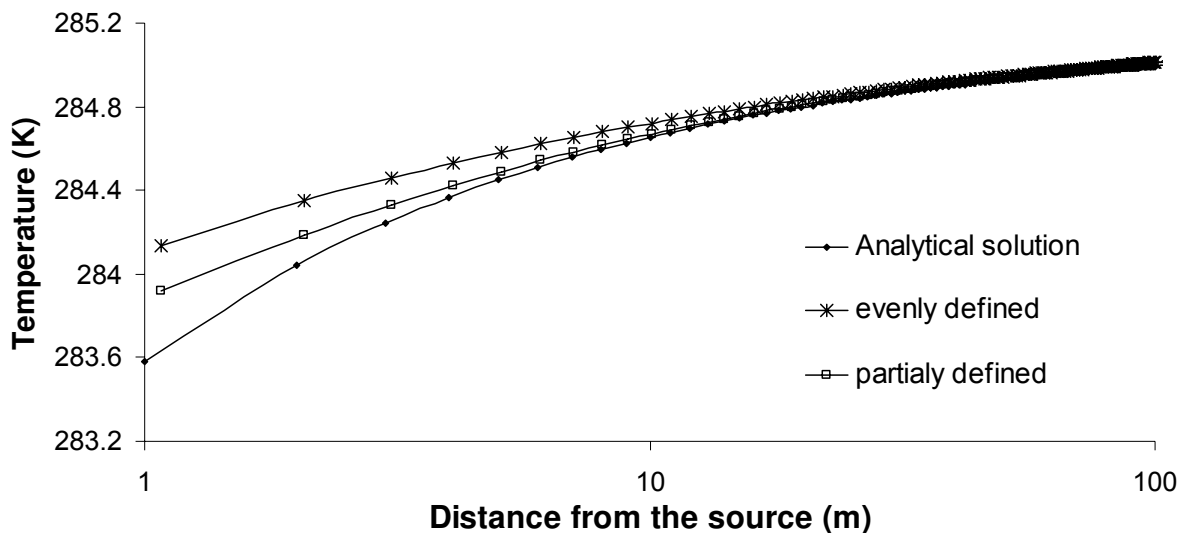
Figure 15. Comparison of numerical results with analytical solution using the multi-diffusion option in MT3DMS. The macrodispersion coefficient is evenly or partially defined in the grid.

For the analysis of the length of the plume and the hydrodynamic dispersion, the results were obtained for the isotherm 185.0 K for 80 days. In Figure 16, the curve of longitudinal dispersivity versus length of the plume can be observed. For this case, when the hydrodynamic dispersion increases, the length of the plume decreases in an almost lineal relation (R^2=0.95). It is important to point out that the length of the plume decreases because energy is extracted from the medium. If energy were injected in the media, an expansion of the plume would be expected.

In the graph, the lineal regression with its equation is included. For the maximum and minimum values, α_h=5 and α_h=1, the length of the plumes are 109 and 208 m, respectively.

From this last, it can be inferred that the longitudinal dispersivity is a sensitive value in the numerical simulation for the used set up.
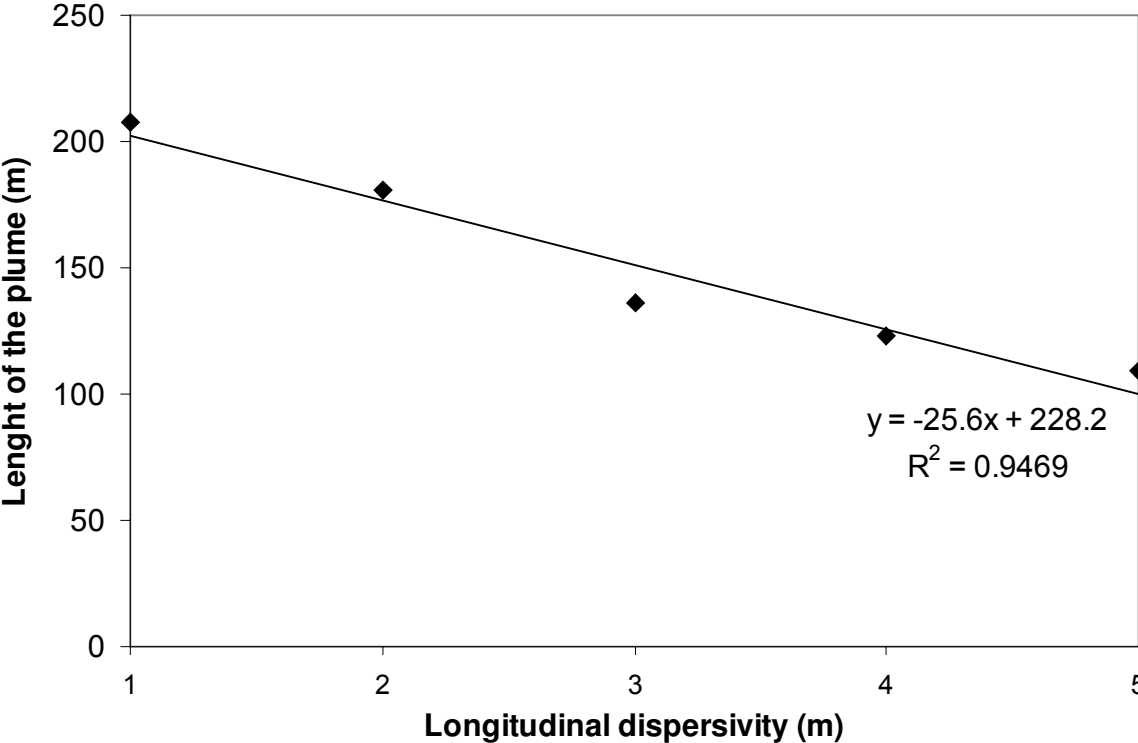
Figure 16. Relation between longitudinal dispersivity and length of the plume.

4 VERIFICATION OF THE USE OF MT3DMS FOR HEAT TRANSPORT SIMULATIONS

4.1 Comparison to results obtained by analytical solutions

In this chapter the numerical results obtained by MT3DMS for heat transport simulations are compared with results attained with analytical solutions for various scenarios. Table 6 lists the scenarios to be simulated based on the dimensionality and the hydraulic gradient. In this table the Peclet number (Pe) is also showed. This number gives a measure of the degree of flow convection in a certain problem. The higher the Pe, the more convection present in the problem. Three main cases are distinguished: conduction dominated problems, $i = 0$ and Pe $=0$; an intermediate problem (conduction/convection), $i = 6.0E-5$ and Pe $=1$, and convection dominated systems, $i = 1.2E-3$ and Pe $=20$.

Table 6. Scenarios test case to be used for the heat transport simulations

Scenarios	Gradient (i)	Steady state (ss) transient (tran)	Darcy´s velocity (v) [m s^{-1}]	Pe	Equation number
2D					
1	0	ss	0.0	0	(19)
2		tran			
3	6.0E-5	ss	4.80E-07	1	(20)
4		tran			(27)
5	1.2E-3	ss	3.69E-05	20	(20)
6		tran			(27)
3D					
7	6.0E-5	ss	4.80E-07	1	(24)
8		tran			(23)
9	1.2E-3	ss	3.69E-05	20	(24)
10		tran			(23)

The analytical solutions are chosen based on the geometry of the source and the dimensionality of the model. Three main analytical solutions and their modification for steady state conditions are used. For the numerical simulation, hypothetical models are simulated in MODFLOW and MT3DMS with the coefficients obtained from the conversions equations (12) to (15).

4.1.1 Input parameter (2D and 3D cases)

The hydrogeological and thermal input parameters to be entered in the numerical codes (MODFLOW and MT3DMS) and also in the analytical solution are listed in Table 7. This dataset was obtained from various sources and a comprehensive study about them can be

found in Hähnlein (2007). The values correspond to consolidated material, for instance, snadstone. Therefore, the verification will be restricted to this type of medium.

Table 7. Hydraulic, geological and thermal input parameters for MODFLOW and MT3DMS

Parameter	Symbol	Value	Unit	MT3DMS	Observation
Density of soil	ρ_s	2650	Kg m^{-3}		
Porosity	n	0.26	-	BTN	
Bulk density	ρ_b	1961	Kg m^{-3}	RCT	
Specific heat capacity soil solid	C_s	880			
Volumetric heat capacity soil	$\rho_s C_s$	2.33E+4	J m^{-3}K		
Volumetric heat capacity water	$\rho_w C_w$	4.19E+4	J m^{-3}K		
Volumetric heat capacity porous medium	$\rho_m C_m$	2.81E+4	J m^{-3}K		
Partition coefficient	K_d	2.10E-4	m^3 kg^{-1}	RCT	
Thermal conductivity	λ_o	2	W (m K)$^{-1}$		
Gradients	i	1.2E-03	-	MODFLOW	
		4.0E-04	-	MODFLOW	
		0.0E+00	-	MODFLOW	
Seepage velocities	v_a	3.69E-05	m s^{-1}	MODFLOW	for i=1.2E-3
		1.85E-06	m s^{-1}	MODFLOW	for i=6.0E-5
		0.00E+00	m s^{-1}	MODFLOW	for i=0
Longitudinal dispersion coefficient	D_x	1.86E-04	m^{2}s^{-1}		for i=1.2E-3
		1.11E-05	m^{2}s^{-1}		for i=6.0E-5
		1.84E-06	m^{2}s^{-1}		for i=0
Horizontal transversal dispersion coefficient	D_y	2.03E-05	m^{2}s^{-1}		for i=1.2E-3
		2.76E-06	m^{2}s^{-1}		for i=6.0E-5
		1.84E-06	m^{2}s^{-1}		for i=0
Vertical Transversal Dispersion coefficient	D_z	3.68E-06	m^{2}s^{-1}		for i=1.2E-3
		1.93E-06	m^{2}s^{-1}		for i=6.0E-5
		1.84E-06	m^{2}s^{-1}		for i=0
Thermal diffusivity	K_T	7.11E-07	m^{2}s^{-1}		Analytical solution
Thermal diffusivity	K_T	1.84E-06	m^{2}s^{-1}	DSP	MT3D
Hydraulic conductivity:	k	8.00E-03	m s^{-1}	MODFLOW	
Retardation factor	R	2.59		RCT	
Initial Temperature ground:	T_o	285.15	K	SSM	
Longitudinal dispersivity:		5	m	DSP	
Horizontal transverse dispersivity:		0.05	m	DSP	
Vertical transverse dispersivity:		0.05	m	DSP	

The column MT3DMS shows the names of the packages in which the respective parameters are entered. The keyword MODFLOW in some parameters indicates that the corresponding value is entered in the groundwater flow model. In the appendix, an example of all input files used for the flow and heat transport simulations can be found.

4.1.2 Efficiencies

In order to quantify the degree of the fit between numerical and analytical solutions, a mathematical method based on match efficiencies of the numerical method regarding to the

analytical solution is used (Loague and Green, 1991). For the subsequent verification the following criteria is used: for efficiencies between 1.00 and 0.98 the match is considered very good, between 0.95 and 0.97, the match is good, and bellow this value down to 0.80 is judged as satisfactory. Results bellow 0.80 down to 0.50 are considered as moderate match. Bellow 0.50 would mean a very high deviation of numerical and analytical result and therefore a comparison would be unnecessary.

4.2 2D-case scenario

4.2.1 Conceptual model

The following scenarios are raised for the 2D case: closed system, steady state and transient conditions for three hydraulic gradients (Table 7). The conceptualization was developed following the findings made in the previous chapter. Figure 17 shows the conceptual model used in this section. It is a one layer model with a grid size of 400 m × 400 m, cell size of 1 × 1 m and a heat extraction source located in one cell with dimensions 0.15 m × 0.15 m. The multidiffusion option in the dispersion package (DSP) is activated. As can be seen in Figure 20, fixed head in the left and right side were specified for the flow model (black columns) using the flow and head boundary package (FHB) of MODFLOW. The source was located in one cell in row 251, column 100.
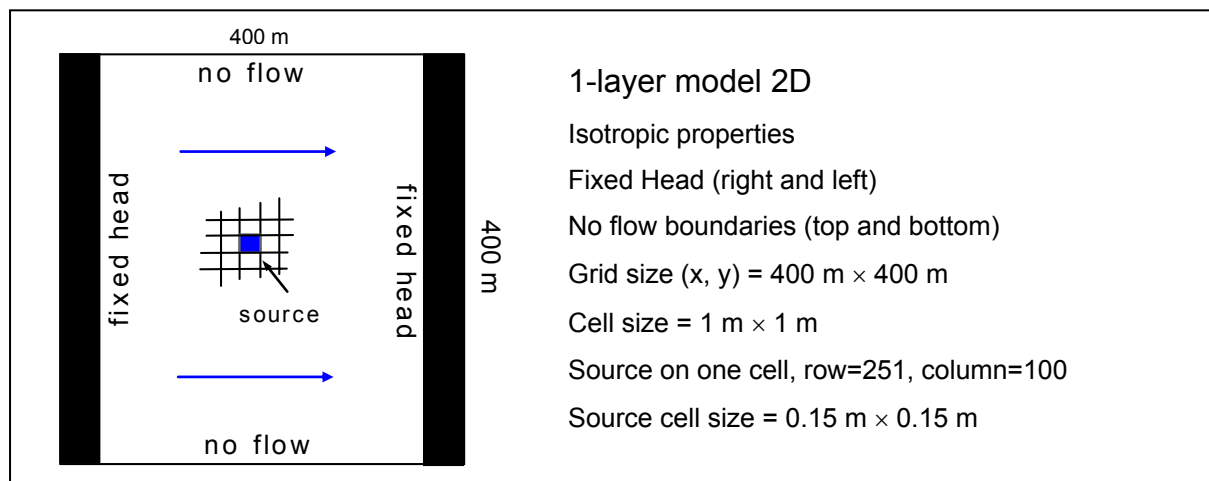
Figure 17. Conceptual model for the 2D test cases, scenarios 1 to 6. Blue square and arrows represent the source cell and flow direction, respectively.

The third order TVD (ULTIMATE) advection solver is used for all the velocities, except $i = 0$ (scenarios 1, 2, 7 and 8). For conduction dominated scenarios, the advection package (ADV) was deactivated. A convergence value of 1.0E-10 and 1.0E-7 for the conduction dominated and convection dominated system, respectively, are assigned in the generalized conjugate

gradient solver package (GCG). The number of outer iterations is set to 100 and for inner iterations to 50.

4.2.2 Method

For each scenario, energy extractions of 60, 100 and 200 W are simulated for 800 days (steady state conditions). For the transient conditions numerical results for 10, 40, 60 and 80 are obtained. The MT3DMS results are compared with the analytical solutions described by the following equation: for gradient $i = 0$, equation number 17 and, for gradients $i = 6.0E-5$ and $i = 1.2E-3$, with equations 18 (steady state) and 21 (transient). To obtain the numerical results, 200 observation points are located on this axis, at the same row as the source cell. Finally, the numerical results will be plotted together with the analytical solution.

4.2.3 Results

In Figure 18, the comparison between the numerical and analytical solutions for gradient $i = 0$ up to 30 m is illustrated (scenario 1). Graph a) shows the temperature profiles along the x-axis for the three energy extractions. The shapes of the curves are quite similar and only a slightly temperature difference between them is noticed throughout the profile. At the cell source the maximum temperature differences occurs and within the first 10 meters, the temperature differences range from 2.7 to 0.2 K for all cases. These is likely due to the source cell size used in MT3DMS (0.15×0.15 m for a BHE) which contrast the definition the infinitesimal point source used in the analytical approach. In graph b), the results in logarithmic scale are depicted. In this graph the temperature difference at 1 m distance from the cell source can be clearly seen. At this point, for the higher energy extraction values, i.e. 100 W and 200 W, the difference between the numerical and analytical solution are 1.4 K and 2.3 K respectively. For 60 W the temperature difference in the same position is 1.4 K. The efficiency for this scenario (0.96) indicates a good fit between numerical and analytical solution (Table 8).

Table 8. Efficiencies for 2D steady state scenarios

Scenario	Efficiency
1	0.96
2	0.99
3	0.92
4	0.59
5	0.99
6	1.00
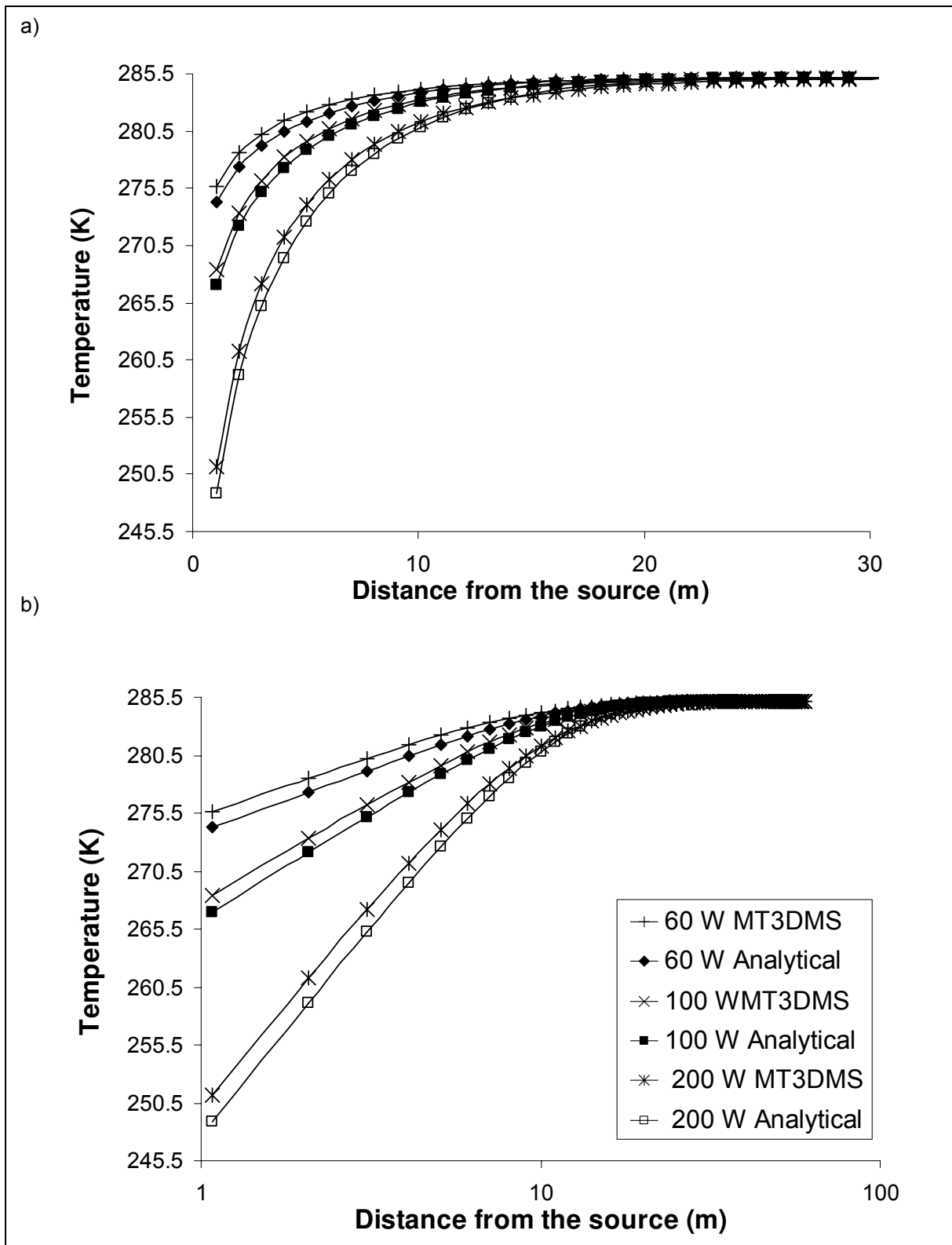
Figure 18. Comparison between 2D numerical and analytical results for gradient *i* = 0, for all energy extractions (60, 100 and 200 W). a) Cartesian x-axis, b), logarithmic x-axis.

Since no flow is present in this system, as the time of energy extraction gets larger or the energy extraction itself is increased, the temperature difference at the source cell gets also larger as has been showed in the results.

It is important to mention that for energy extractions of 100 and 200 W at a distance below approximately 10 meters from the source, the numerical results are beneath the freezing point of water (273.15 K). Although using these energy extractions lead to a freezing of the ground water near the BHE, they are used in this investigation as hypothetical scenarios to exaggerate the temperature difference of the media. This is also observed for the other gradients in the subsequent analyses.

Figure 19 shows the comparisons of the analytical and numerical results for transient condition (10, 20, 40 and 80 days) for the three energy extractions.
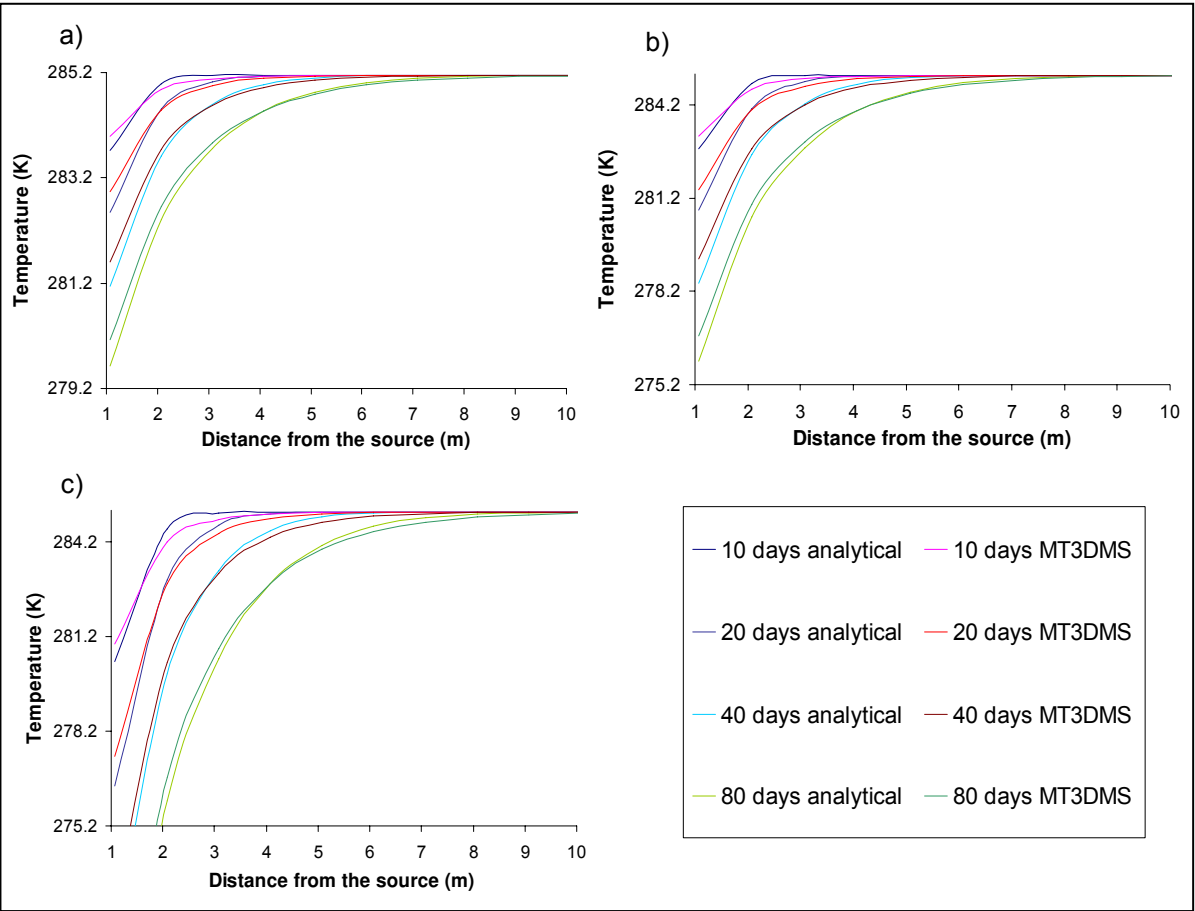
Figure 19. Comparison between numerical and analytical results for transient conditions (10, 20, 40 and 80 days) for gradient *i* = 0. a) Energy extraction 60 W, b) 100 W and c) 200 W.

Two important behaviours are observed in these graphs. As the length of the stress periods gets larger, the match between numerical and analytical results improves for all energy extractions and a temperature decrease at the cell source is observed. The efficiency for all energy extraction for 40 days is 0.99 (Table 8, scenario 2).

In the next two pages, the numerical and analytical results for scenarios 3 and 5 are shown in Figures 20 and 21, respectively. For gradient, *i* = 6.0E-5, despite the large temperature

difference observed, the trend of each pair of curves are similar with an efficiency of 0.92 (Table 8).
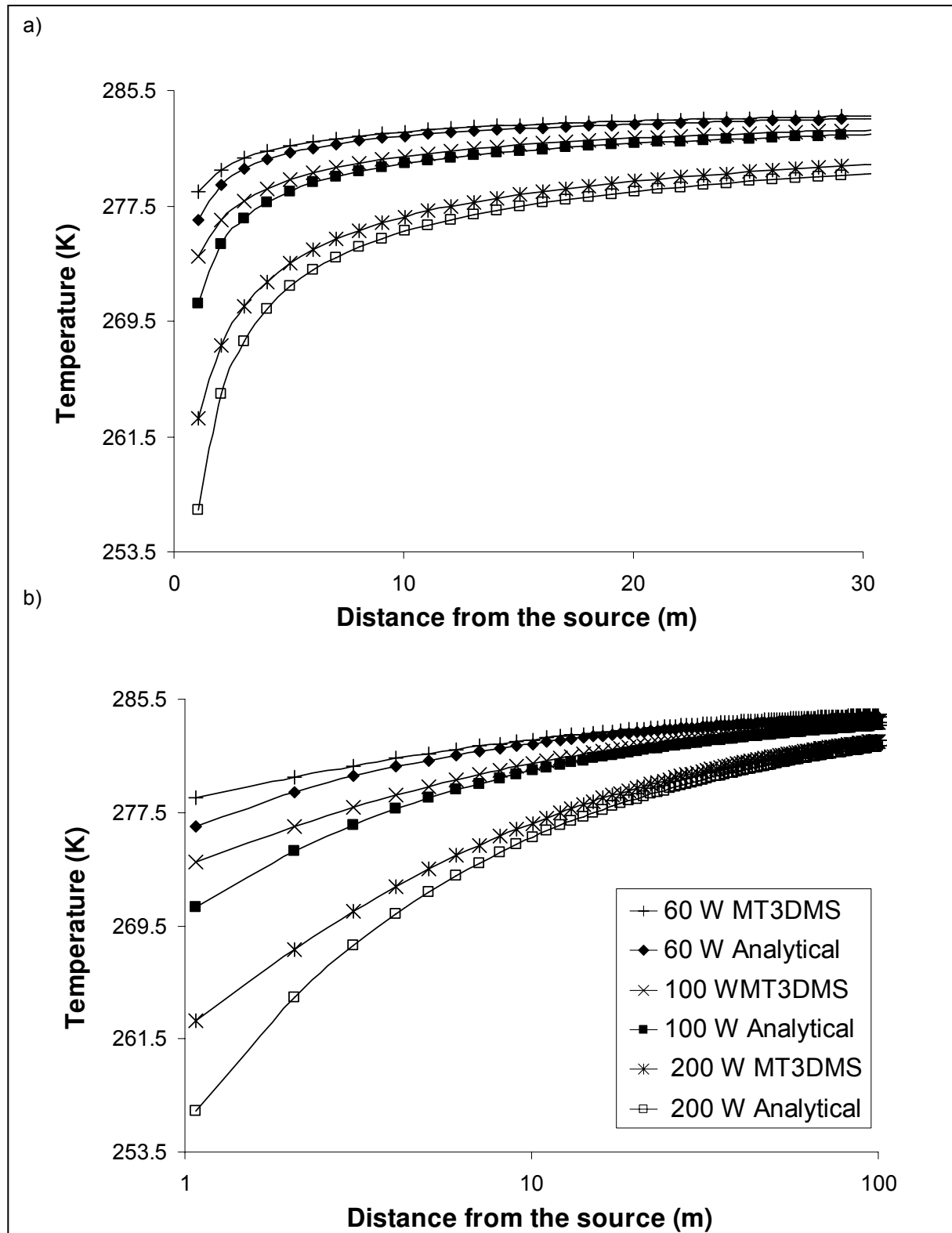
Figure 20. Comparison between numerical and analytical results for gradient *i* = 6.0E-5, for all energy extractions (60, 100 and 200 W). a) cartesian x-axis, b) logarithmic x-axis.
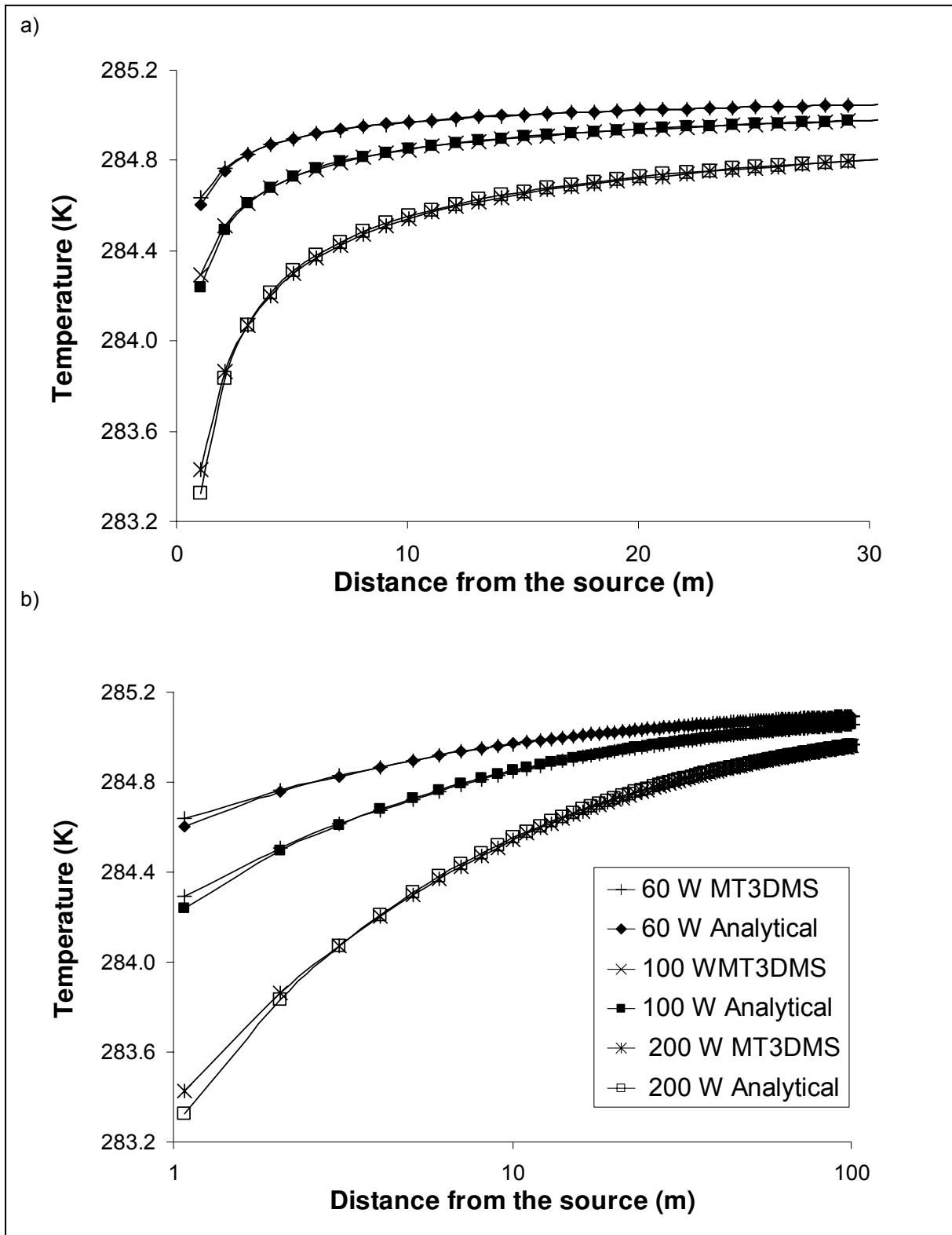
Figure 21. Comparison between numerical and analytical results for gradient *i* = 1.2e-3, for all energy extractions. a) cartesian x-axis, b) logarithmic x-axis.

On the other hand, for i = 1.2E-3, an efficiency of 0.99 was obtained which indicates a very good match between numerical and analytical solution. For this gradient, the curves almost overlapped each others throughout the entire plume centreline, only near the source temperature differences are found. This error is due to the size of the source cell, while in the

analytical solution it is an infinitesimal line, in the numerical code, the size of a BHE are used for the simulations (0.15 m × 0.15 m).

Once again, as the energy extraction increases, the temperature at the cell source decreases considerably. Comparing Figures 20 and 21, it can be noticed that for the highest gradient the match between numerical and analytical solution is much better than that for the lowest gradient. This situation is likely related to either a limitation of the analytical solution for low hydraulic gradients or a decrease of accuracy of the code for this type of gradients.
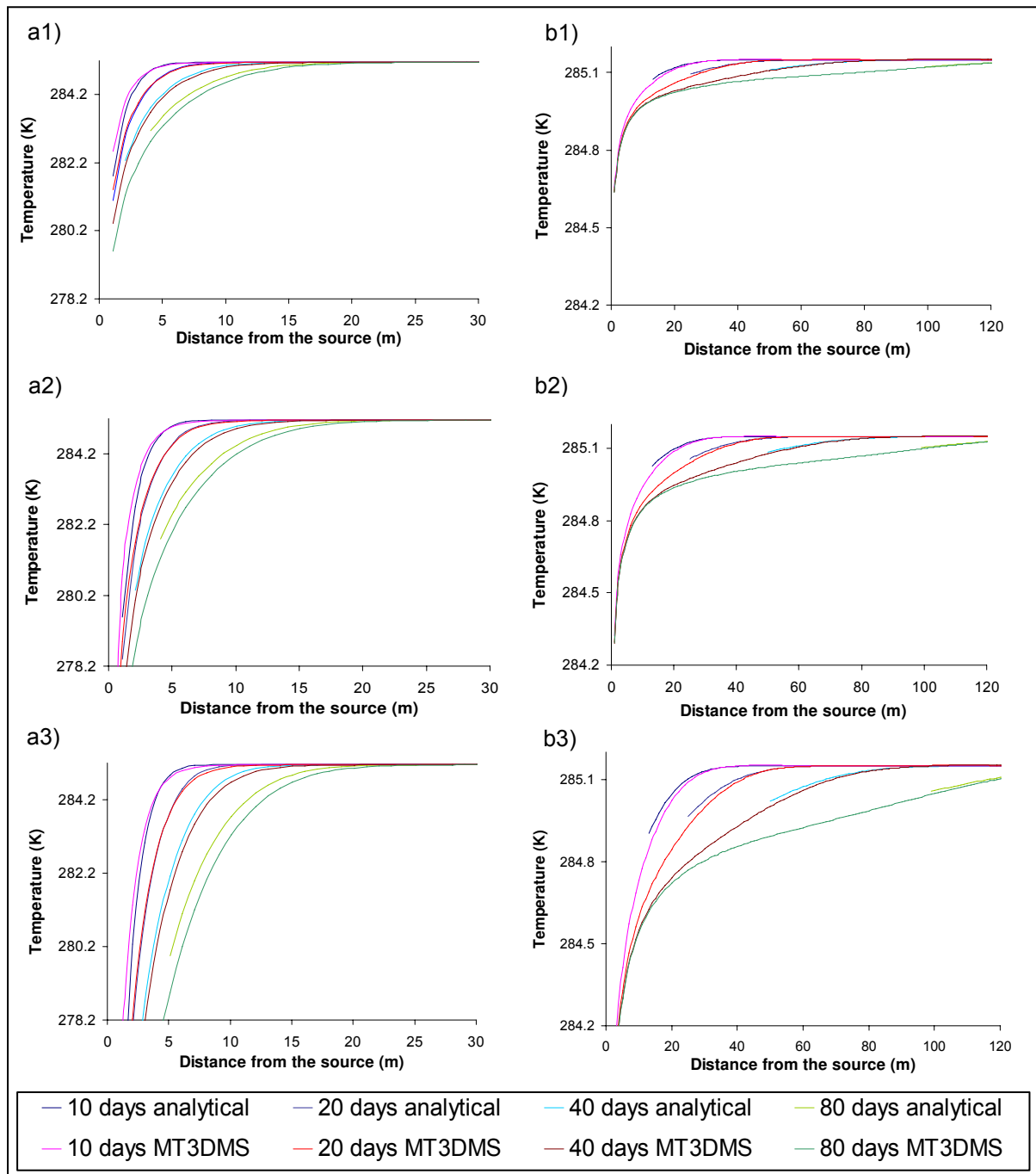
Figure 22. Comparison between numerical and analytical results for transient conditions. Left side: *i* = 6.0e-5 for energy extractions: a1) 60 W, a2) 100W and a3) 200. Right side, *i* = 1.2e-3 same energy extraction (b1, b2 and b3).

The results for transient conditions for both gradients are showed in Figure 22. The graphs a1) to a3) (left side on figure) show the comparison of numerical and analytical results for i = 6.0E-5. Graph b1 to b3 (right side) depict the comparison for i = 1.2E-3.

For the lowest gradient, the match between numerical and analytical curves has an efficiency of 0.53 for 40 days, for all energy extractions, this indicates a low fit between the curve. For the highest gradient, as the length of the stress period gets higher, the match of the curves improves. For this gradient a very good match for all energy extraction can be observed (efficiency of 1.0).

Figures 23 shows visualizations of the heat plume for gradients, a) i = 0, b) i = 6.0E-5 and c) i = 1.2E-3, generated with the software MODEL VIEWER. The images are for an energy extraction of 60 W.
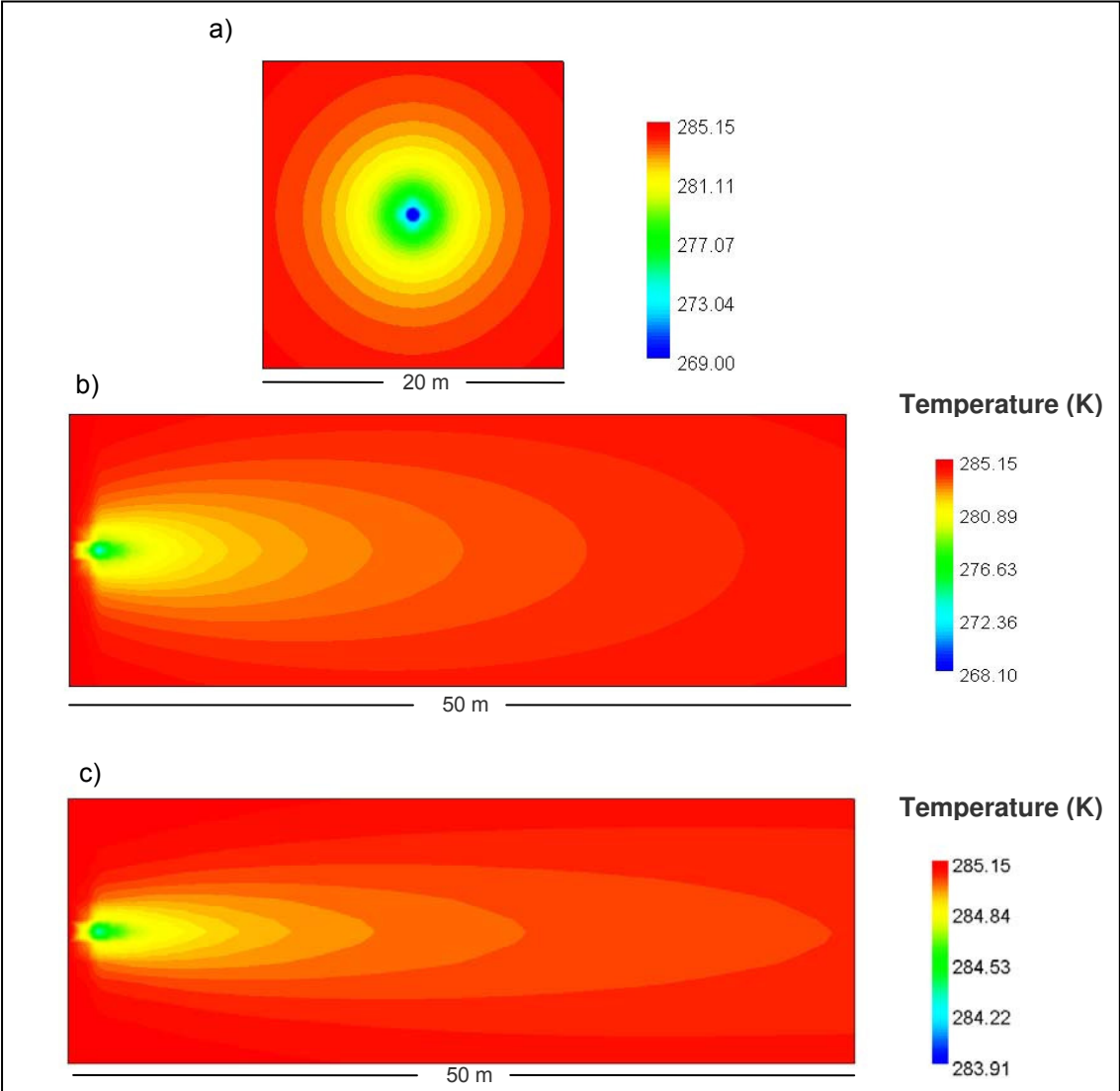
Figure 23. 2D illustrations of the heat plume for an energy extraction of 60 W. For various gradients: a) i = 0, b) i = 6.0E-5 and c) i = 1.2E-3.

It can be clearly seen that the higher the gradient, the larger the plume downgradient. On the other hand, after 800 days the temperature at the source cell for the conduction dominated and the intermediate problems are lower that for the advection dominated problem. For no flow situation, the temperature at the source cell after 800 days is 212.46 K while for the intermediate and the convection dominated situation, the values are 240.67 and 281.04 K, respectively (This temperatures are not in the range presented in the figures due to limitations of the visualization tool). It means that the groundwater passing trough the source cell carrying energy tends to stabilize the systems leading to a small change in temperature at the source point and therefore smaller cold plumes.

4.3 3D-case scenarios

4.3.1 Conceptual model

In Figure 24, the conceptual model for the 3D case is shown. The scenarios for this case are: closed system for steady state and transient conditions. As for the 2D case, the configurations of each case are done based on the results obtained in chapter number 3. For the 3D case, these features are: grid size of 400 m × 400 m, 9-layers model, area of the source (x, y-axes) 0.15 m × 0.15 m in one cell, and thickness of 3 m (3 cells, 1 meter each).
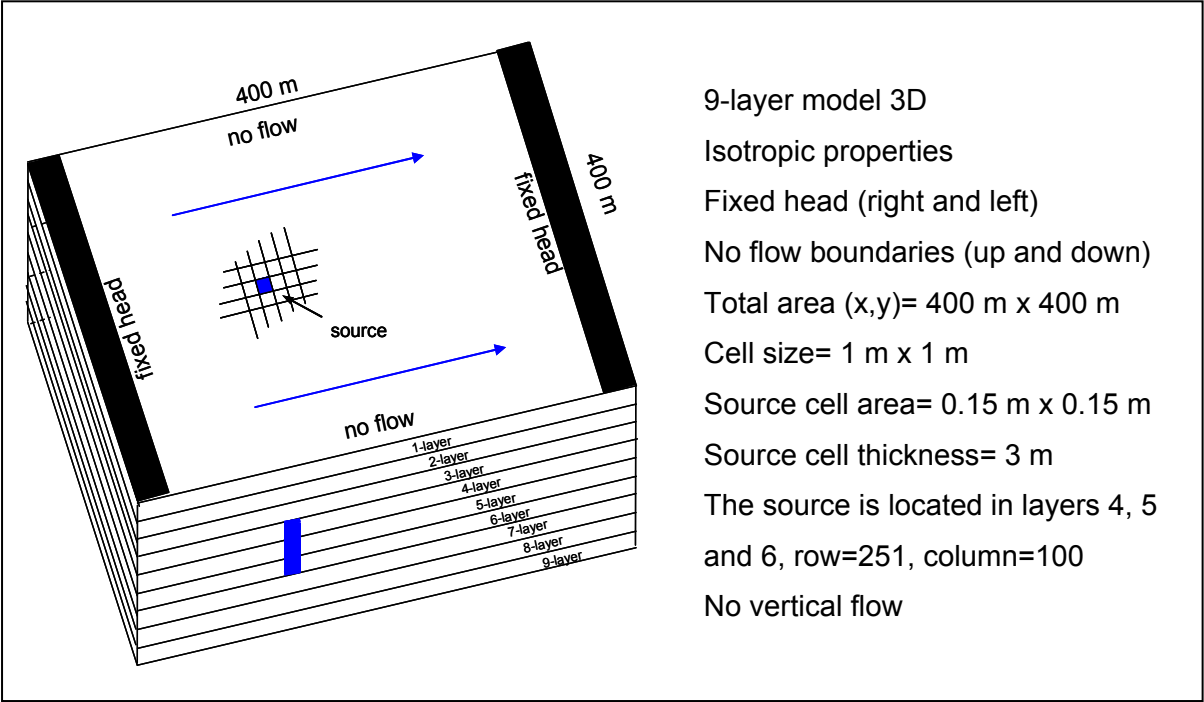
Figure 24. Conceptual model for the 3D test cases, scenarios 7 to 10. Blue square and arrows represent the source cell and flow direction respectively. The source is located in 3 cells in layers 4, 5 and 6.

4.3.2 Method

For this 3D analysis, the same approach will be used as for the 2D case. Three main scenarios are considered for steady state and transient conditions. The results from MT3DMS are compared to the results obtained by the analytical solutions for planar source (equations 21 and 22).

4.3.3 Results

The comparisons between the numerical and analytical results for the gradient i = 6.0E-5 for the three energy extractions are shown in Figure 25. In graph a), the temperature profile along the x-axis up to 50 meters for the fifth layer can be seen. Near the source (1 m approximately), the maximum temperature difference was found. In spite of this difference, there is a satisfactory match between the numerical and the analytical curve for each energy extraction with an efficiency value of 0.80 (Table 9). In Figure 25 b), the results in logarithmic scale (x-axis) are shown. In this illustration, the differences in the first meters are much better visualized. Within the 2 first meters approximately, a large difference between numerical and analytical results is observed. In the same way, between 3 meters and 12 meters, there is again a markedly difference between both results. As the energy extraction is increased, the difference between the simulated and mathematical data increases, particularly the initial temperature at 1 meter distance from the source. Nevertheless, the curves still stand the shape and the trend (efficiency of 0.80).

In Figure 26, the comparisons of the numerical and analytical results for the gradient i = 1.2E-3 and the three energy extractions are depicted. Contrary to the previous gradient, the temperature profile for the numerical and analytical results have a good match along the profile with an efficiency of 0.96. In Figure 26 b), it can be seen that the differences between the numerical and analytical solutions at 1 m from the source are very low. The efficiency for this gradient was 0.96 which indicates a good match between numerical and analytical solutions.

For the gradient i = 1.2E-3, the difference between numerical and analytical solutions is lower than for gradient i = 6.0E-5. For instance, at 1 meter distance from the source, the differences between numerical and mathematical curves are: 0.25 K, 0.20 K and 0.1 K for 200 W, 100 W and 60 W, energy extraction respectively. On the other hand, for the gradient i = 6.0E-5, these differences are: 4 K, 2 K and 1 K, for 200 W, 100 W and 60 W, respectively.

Table 9. Efficiencies for 3D steady state scenarios

Scenario	Efficiency
7	0.80
8	0.87
9	0.96
10	0.98

Another important feature is the temperature difference near the source (at 1 m). As the energy extraction increases, the temperature at this point decreases considerably. For $i = 6.0E-5$, 60 W, it is 281.724 K, while for 200 W, it is 273.697 K, a difference of 8.027 K. On the other hand, for $i = 1.2E-3$, the temperatures at 1 meter from the source are, 283.414 K and 279.340 K for 60 and 200 W, respectively. It is a total difference of 3.8 K. This small temperature difference obtained for the highest gradient, indicates that even if the energy extraction is increased, the energy carried by the groundwater passing through the BHE regularized the temperature at this location and downgradient.
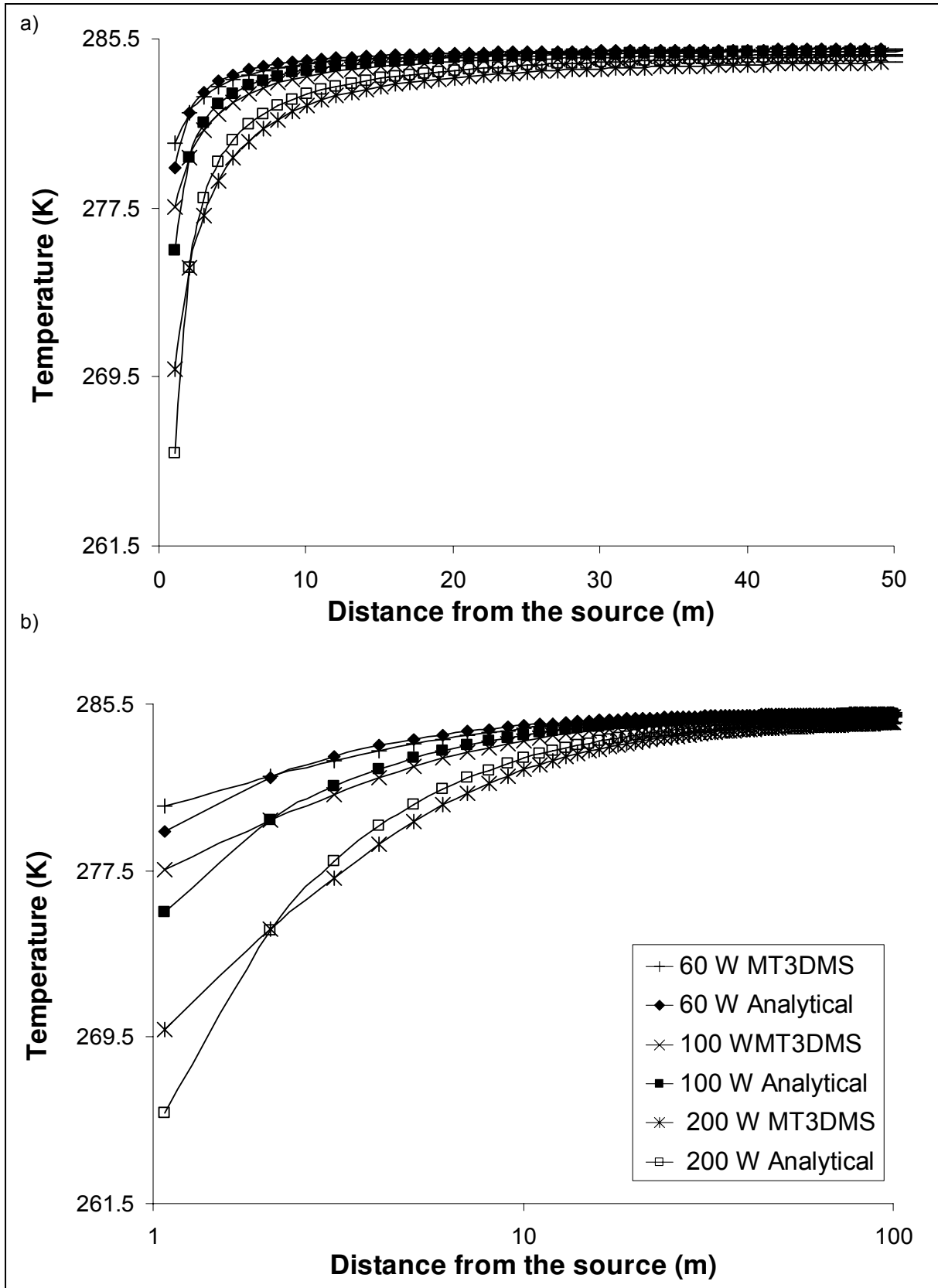
Figure 25. Comparison between numerical and analytical results for gradient *i* = 6.0E-5, for all energy extractions. a) cartesian x-axis, downer graph, logarithmic x-axis.
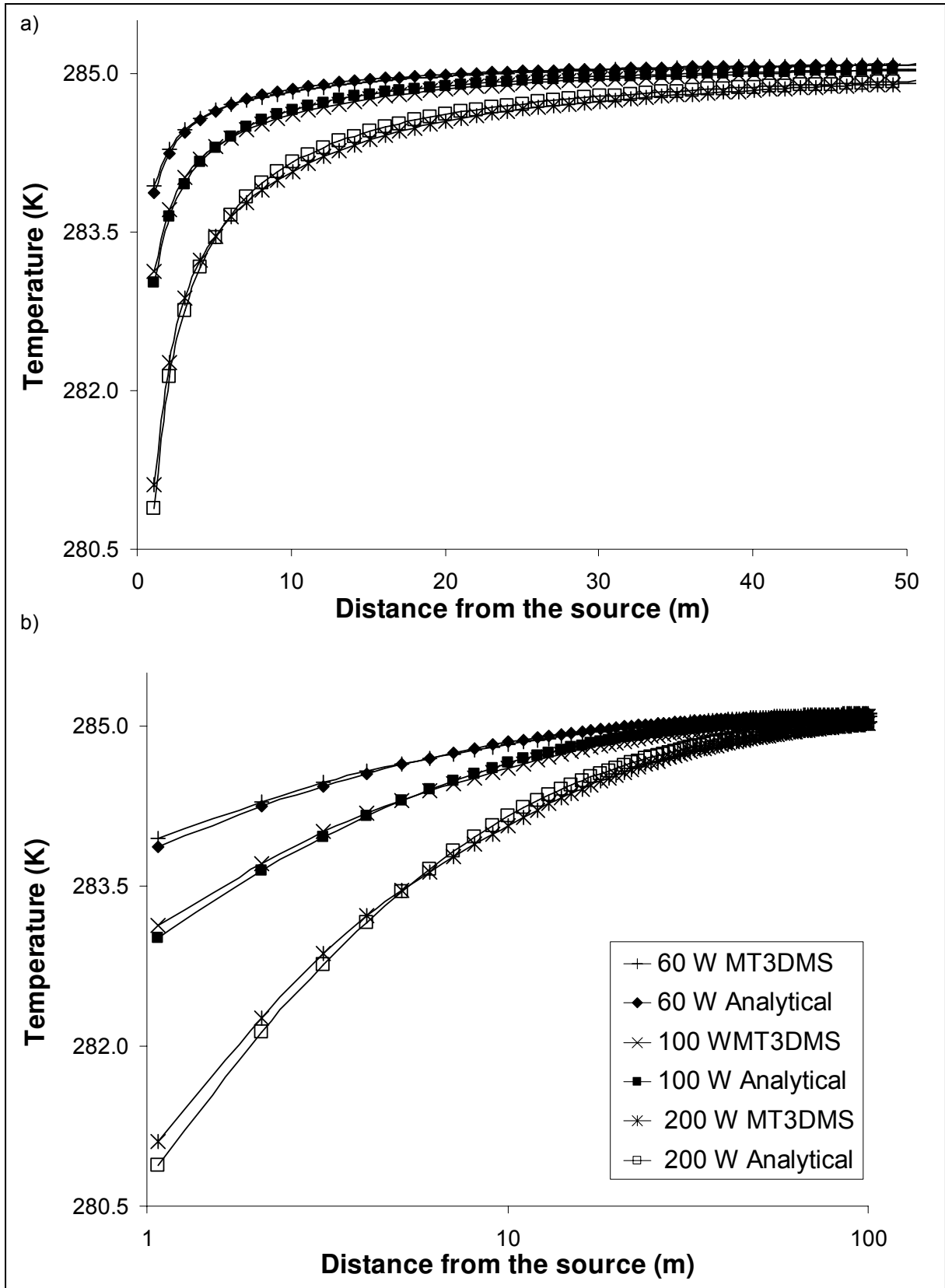
Figure 26. Comparison between numerical and analytical results for gradient *i* = 1.2e-3, for all energy extractions.

For the transient conditions the results are illustrated in Figure 27, which shows the comparison of each gradient and each energy extraction with the respective analytical solution for 10, 20, 40 and 80 days.
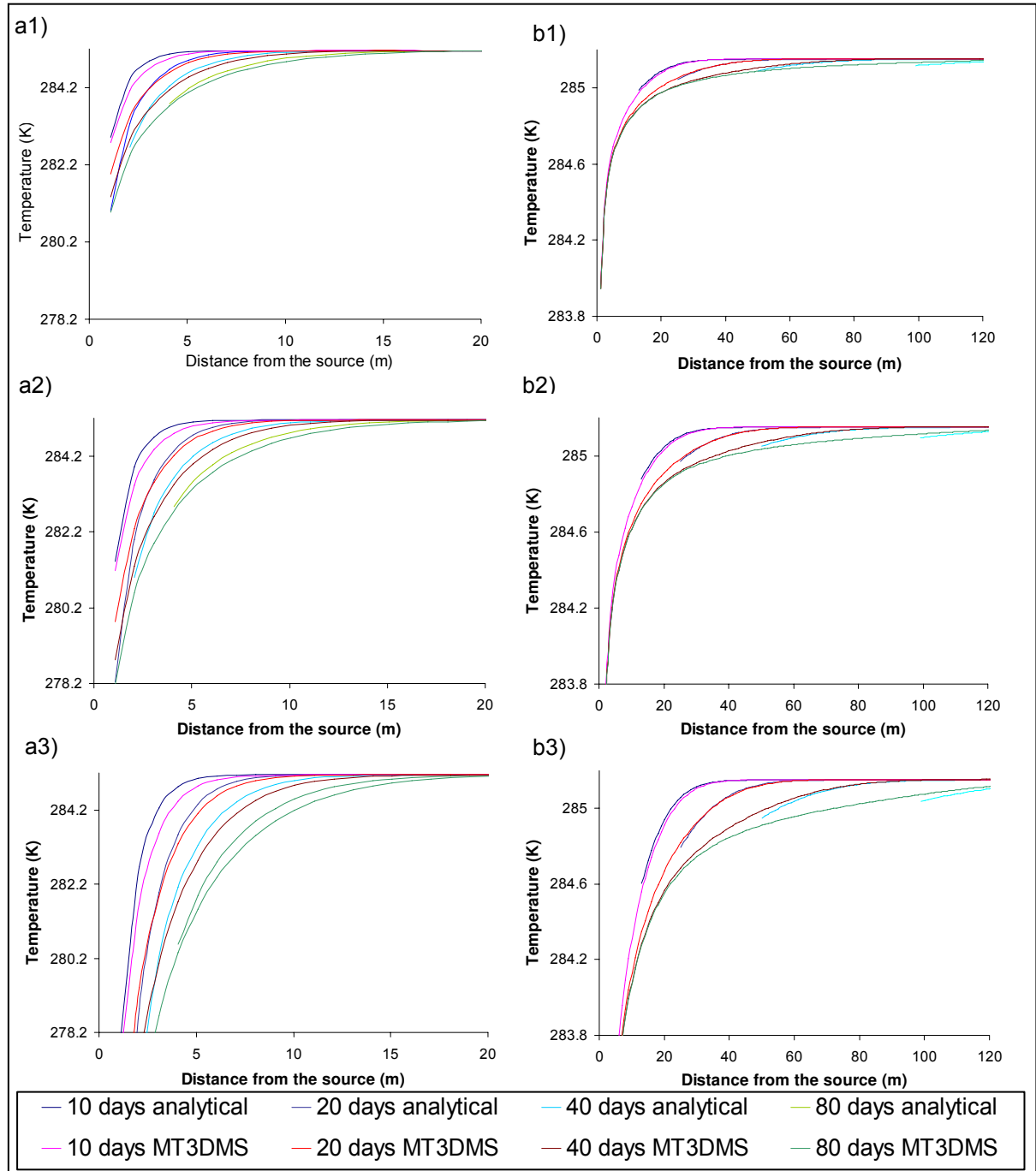
Figure 27. Comparison between numerical and analytical results for transient conditions. Left side: i=6.0e-5 for energy extractions: a1) 60 W, a2) 100W and a3) 200. Right side, i=1.2e-3 same energy extraction (b1, b2 and b3).

In the left side of Figure 27 (graphs a1, a2 and a3), the comparison corresponding to $i = 6.0E$-5 are showed for all energy extractions (increasing downwards). In the right side (graphs b1, b2 and b3), there are the comparison for $i = 1.2e$-3. The match between the numerical and

analytical curves for gradient i = 6.0E-5 is satisfactory with an efficiency of 0.87, but they begin to differ as the energy extraction increases. That can be seen in Figure 27, graph a3 (200 W), where a large temperature difference between 5 and 20 m is found. For gradient i = 1.2E-3, the match between both curves is quite good for all energy extraction (efficiency of 0.98). However, a slightly difference for 80 days can still be appreciated.

At 1 m from the source, as the energy extraction increases, the temperature at this point decreases markedly, for instance, for i = 6.0E-5, after 80 days, the following decreased is observed: 281.7 K, 279.4 K and 273.6 K (out of the scale in the graph), for 60, 100 and 200 W, respectively. On the other hand, for i = 1.2E-3 after 80 days, temperatures at 1 m distance from the source are 283.4 K, 282.2 K and 279.3 K for energy extractions of 60, 100 and 200 W respectively.

In Figure 28, 3D illustrations for an energy extraction of 60 W are depicted. The results are for a stress period length of 800 days. Figure 28 a) shows the heat plume downgradient for gradient i = 6.0E-5. Figure 28 b) depicts the heat plume for i = 1.2E-3. As for the 2D case, the same behaviours are observed
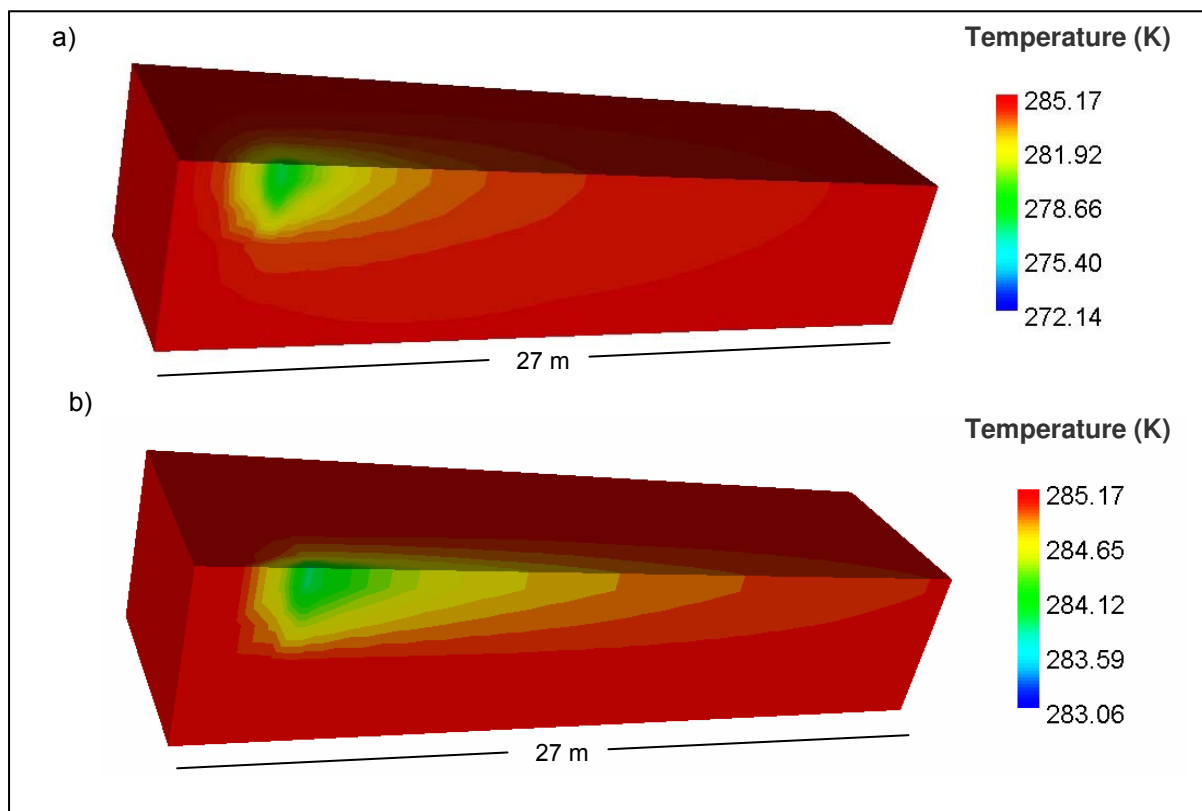
Figure 28. 3D illustrations of the heat plume for an energy extraction of 60 W. For various gradients: a) i=0, b) i = 6.0E-5 and c) i = 1.2E-3.

4.4 Comparison to alternative numerical solution

In this section the MT3DMS results are compared with results obtained with the numerical code SHEMAT (Clauser, 2003). This commercial software is also based on the numerical method finite differences and it is widely used in the geothermal modelling area (Clauser, 2003; Kühn et al., 2004; Pape et al., 2005; Rühaak et al., 2008). The code MT3DMS was also verified with other commercial numerical code FEFLOW (Diersch, 2002). The verification and analyses for similar scenarios can be found in the thesis "Numerical Verification of Shallow Geothermal Models Using FEFLOW" (Pejman, 2008). This work is part of the same working group at the ZAG of the University of Tübingen. In this investigation sensitivity analyses are presented of some key parameters as: hydraulic conductivity, longitudinal dispersivity among others.

4.4.1 Method

The conceptual model is the same used for the 2D case depicted in Figure 19. The simulation with SHEMAT is performed for gradient $i = 4.0\text{E-}4$ (Pe =7) and steady state conditions. As for the MT3DMS simulations, three energy extractions (60, 100 and 200 W) are applied in one cell. The following options and input parameters are used in SHEMAT:

- Advection algorithm: upwind
- The flow simulation is not temperature dependent
- Stress period length = 800 days
- Converge limits: flow = 1E-4, heat = 1E-2
- Reference density = 999.7 kg m^{-3}

The additional input parameters for the flow and heat model are the same used for the previous section (Table 7). The SHEMAT results are obtained with 100 observation points located along the x-axis as in MT3DMS. They are processed with a MATLAB routine and later brought in EXCEL, with which the comparison and graphs are elaborated.

4.4.2 Results

Figure 29 shows the MT3DMS and SHEMAT numerical results for the three energy extractions. As can be seen, there is a slightly temperature difference between the results within the first 10 m distance from the source. At 1 m from the source, the difference is of about 0.4 K for all energy extractions. For distance between 10 m and 100 m, the match between both numerical curves is reasonably good.
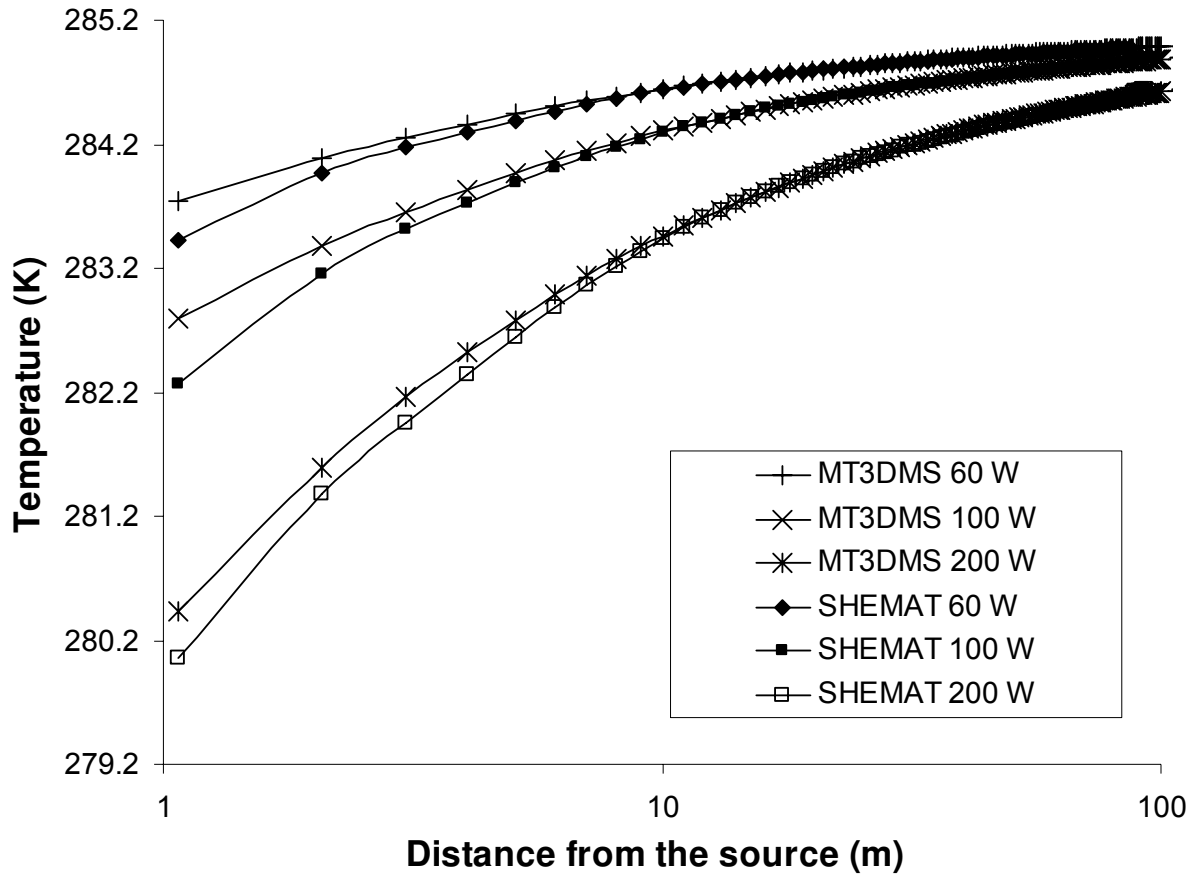
Figure 29. Comparison between MT3DMS and SHEMAT results for i=4.0E-4 and three values of energy extraction (60, 100 and 200 W).

The visualization of the heat plumes obtained by the two codes is showed in Figure 30. Graph a) depicts the heat plume simulated by MT3DMS and, graph b) shows the heat plume calculated by SHEMAT. These graph are only illustrative, with them a quantitative analysis can not be done.
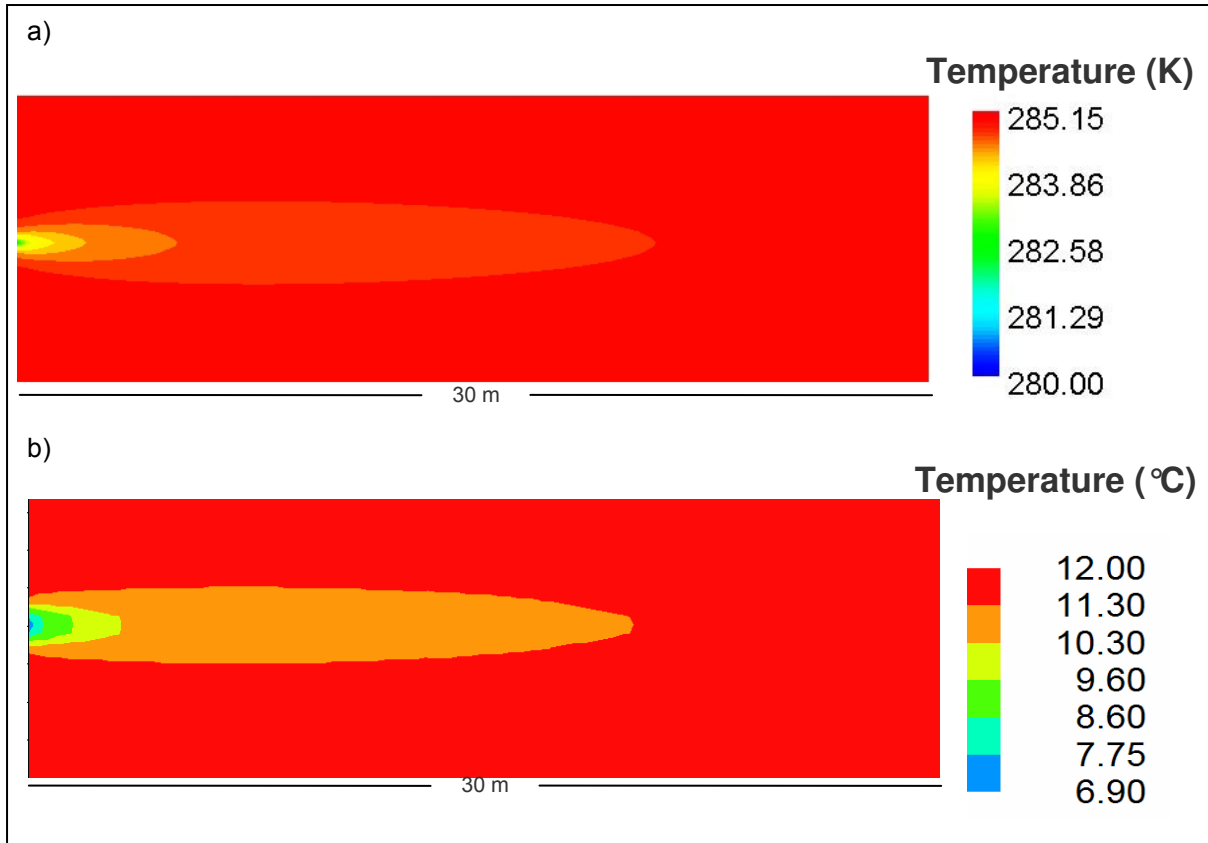
Figure 30. 2D illustrations of the heat plumes for an energy extraction of 60 W. a) Generated by MT3DMS and b) by SHEMAT. SHEMAT results are in centigrade degrees (°C) and the colour scale slightly differs than that from MODEL VIEVER.

5 CONCLUSIONS

In the current study it could be demonstrated that the numerical code MT3DMS has the potential to be applied for heat transport simulations, however until now care has to be taken with the results close to the source (< 10 m). The adaptation of the code does not depend only on the exchange of the conforming coefficient of the heat and solute transport equation but also on the appropriate model set. Furthermore, the use of particular options of the code such as the multidiffusion option, or the type of advection solver, allows better modeling of a certain problem.

For simulating BHEs of GSHP systems close to a real situation, it was necessary to find out the response of the code to some of the key feature of these systems such as: grid size, type of solver to be used depending on the flow velocity, discretization at the cell source and definition of the macrodispersion coefficient.

Regarding the grid size, it was stated that heat simulation of BHEs can be performed for sizes ranging from 200 m × 200 m to 1000 m × 1000 m (or even larger) without getting any boundary effect. However, for 3D representations, as the grid size got larger than 700x700 m the results began to differ from the analytical solutions due to the inclusion of a regional effect in the numerical result. This regional effect leads to a non-physical smoothing out of the response of the media to the extracted energy. Therefore grids equal or larger than this size must be avoided for heat transport simulations of a single BHE. From a qualitative point of view, grid sizes smaller than 200x200 m should also be avoided. In the vertical extension for 3D models, a minimum of 7 layers or at least 7 m should be used to avoid the boundary effects of the surface and/or the bottom layer.

An important aspect when using MT3DMS either for heat or solute transport simulation is the selection of the type of solver depending on the flow velocity. In the analysis, it was found out that the third order TVD or ULTIMATE method was the most accurate solver, with a good match for all the gradients ($i = 6.0E-5$, $i = 4.0E-4$ and $i = 1.2E-3$). Nevertheless, it needed the larger execution time for the simulation in all cases. The method of characteristics also showed good results and moreover, the running time was shorter. For this method, a number of moving particles per cell must be entered in order to allow the calculations. The selection of how many particles to use in a simulation can be a complex task. Even the simulation can stop if this number is not large enough. This is not necessary for the ULTIMATE scheme.

Therefore, this method was used throughout the investigation. However, all solvers showed a good approach for all gradients, except the finite difference method, which only got satisfactory results for i = 4.0E-4 (Pe =7). Thus, the selection of the solver depends on the needs of the modeler regarding accuracy and running time.

Decreasing the cell source size in the numerical model resulted in an improvement of the match between numerical and analytical results. Since a BHE has diameters less or equal than 0.15 m, it was of major importance to include this feature in the simulation. Effectively, as the source cell size was decreased, the match between the numerical and analytical curves improved noticeably, with the best being the source cell size of 0.15 m × 0.15 m. It is worth to mention that although discretizations around the source cell were not deeply investigated, it was found out in preliminary simulations that if some cells close to the source are discretized, the results can improve to some extent. Molina 2008, applied a discretization around the source cell to similar conceptual models as used here, which led to an improvement in the fit efficiency of the MT3DMS results with 5 analytical solutions. Although, during this investigation we tried to find a procedure for the discretization near the extraction cell, there is not a precise method for determining this important step and we presumed that it depends on either the expertise of the modeler or/and the characteristics of a certain problem.

Differences between analytical and numerical solutions observed in the first stages of the investigation were partly due to upgradient effects near the source (Grathwohl, personal communication). However, a recipe was found to avoid this effect using the multidiffusion option included in MT3DMS. With this option the upgradient effect could be reduced and the heat transport was mainly considered downgradient. Using this option the match between numerical and analytical results improved significantly. However, upgradient effect at 1 m for the source is still happening. Although physically, heat dissipation upgradient is present in the media, for comparing the numerical results with the analytical solution, it is required to decrease this phenomenon.

The application of the MT3DMS code for heat transport simulation was verified using analytical solutions and the numerical simulation package SHEMAT. The conceptualization for the verification process was raised based on the results obtained in the chapter number 3 of this thesis. For all gradients (i = 0, i = 6.0E-5 and i = 1.2E-3) in 2D and 3D models, the match efficiencies range between 0.80 and 1.00 indicating satisfactory, good and very good fits. Moreover, for the applied energy extractions (60, 100 and 200 W), high efficiencies were obtained. The match between the results improved when the period length was larger and it

reached its best result for steady state conditions. For the highest flow velocities it was noticed that the temperature change around the borehole was lowered and therefore the cold plume developed downgradient was shorter. It is due to the energy supplied by the higher amount of water passing through the BHE.

From 1 to 10 m distance from the source, there are cases where the matches between 2D and 3D analytical and numerical results slightly differed. These differences can be lowered using discretizations around the source cell (Molina, 2008). As it was mention above, there is not a procedure for discretizing near the source and in most cases a trial and error approach can be helpful.

Of particular interest was the gradient i = 6.0E-5. This scenario has a Pe =1 and it is a so-called intermediate problem (convection/conduction). For this gradient the lowest match efficiency was found (0.92 for the 2D case and 0.80 for the 3D case), with large differences near the source, particularly on the 3D model. This is possible due to a limitation of the analytical solution for low gradients or a decrease in accuracy of the MT3DMS code. Likewise, the high longitudinal dispersivity (α_h=5) used for the simulation could lead the numerical method to obtain inaccurate results.

The scenario compared with the numerical results obtained by SHEMAT was i = 4.0E-4, Pe = 7. Also a good match between both numerical methods was found. Only within 10 m distance from the source, a faint difference between the curves was observed. The highest value of this difference is 0.4 K at 1 m from the source but it decreased for larger distances. In spite of this difference, we can conclude that the MT3DMS code was effectively verified with SHEMAT, which is a well known and usually applied numerical code for geothermal assessments.

Finally we can concluded that throughout this investigation, the application of the numerical code MT3DMS for 2D and 3D heat transport simulations was verified. Moreover, we deepened the understanding of not only the application but the capabilities of the code for heat simulation. Nevertheless, the code design does not include some important features that have to be considered for heat transport simulations, such as: temperature dependency of some input parameters as longitudinal conductivity or density of the water. For the expanding area of shallow geothermal investigations, the availability of such a free and easy to use numerical code represents a suitable element to work with.

There are still many open issues that need to be investigated in order to completely develop the MT3DMS code for heat transport modelling. For shallow geothermal systems, the exchange with the atmosphere, i.e. with the surface, is an important aspect. To date, the use of MT3DMS was done for confined aquifers without taking into account unsaturated layers. Although, MT3DMS can be used for solute transport in unconfined aquifers, for applying the code for heat transport simulation a subroutine must be developed based on the equation (16). For time restriction this task was not included in the present thesis, but it will be one of the upcoming objectives of the research group. Likewise, open systems were not studied in this investigation, since there is already a compilation of analytical solution that can be used to verify the model for these systems.

6 REFERENCES

Alabama University (2007). MT3DMS − A modular 3-D multi-species transport model for simulation of advection, dispersion and chemical reactions of contaminants in groundwater systems. Hydrogeology group. Accessed on June, 2007, at http://hydro.geo.ua.edu/mt3d/

Brehm D. (1989). Development, validation and application of a 3-dimensional, coupled flow and transport finite differences model. Lenz-Verlag, Giessen. 84 p.

Carslaw, H.S. and Jäger, J.C. (1959). Conduction of Heat in Solids, second ed. Oxford University Press, Oxford, UK, 510 p.

Cathomen, N., (2002). Wärmetransport im Grundwasser − Auswirkung von Wärmepumpenanlagen auf die Grundwassertemperatur am Beispiel der Gemeinde Altach im Vorarlberger Rheintal. Diplomarbeit. ETH Zürich.

Clauser, C. (1988). Opacity the Concept of Radioactive Thermal Conductivity. In: R. Hänel, L. Rybach & L. Stegena, Handbook of Terrestrial Heat Flow Density Determination, Kluwer, Dordrecht, p. 143-165.

Clauser, C. (2003). Numerical Simulation of Reactive Flow in Hot Aquifers, SHEMAT and Processing SHEMAT. Springer, Berlin-Heidelberg.

Clauser, C. (2006). Geothermal Energy, In: K. Heinloth (Ed), Landolt-Börnstein − Numerical Data and Functional Relationships, New series, vol. 8: Energy Technologies, Subvolume 3: Renewable Energies, Springer Verlag, Heidelberg-Berlin.

Diao, N, Li, Q and Zhaohong F. (2004). Heat transfer in ground heat exchangers with groundwater advection. International Journal of Thermal Sciences, vol. 43, p. 1203-1211.

Diersch, H.J.G., (2002). FEFLOW 5- User's Manual. WASY GmbH, Berlin.

Domenico, P. A., and Robbins, G. A. (1985). A new method of contaminant plume analysis: Ground Water, vol. 23, issue. 4, p. 476-485.

Ferguson G. (2007). Heterogeneity and thermal modelling of ground water. Ground Water, vol. 45, issue. 4, p. 485-490.

Fried J.J., Muntzer, P. and Zilliox, L. (1979). Ground-water pollution by transfer of oil hydrocarbons, Ground Water, vol. 17, issue 6, p. 586-594.

Hähnlein, S. (2007). Rechtliche Grundlagen und Ausdehnung von Kältefahnene bei Erdwärmesonden. Diplomarbeit. Institut für Geowissenschaften. Zentrum für Angewandte Geowissenschaften, Universität Tübingen. Germany.

Harbaugh, A.W., Banta, E.R., Hill, M.C., and McDonald, M.G. (2000). MODFLOW-2000, the U.S. Geological Survey modular ground-water model -- User guide to modularization concepts and the Ground-Water Flow Process: U.S. Geological Survey Open-File Report 00-92, 121 p.

Holzbecher, E. (1998). Modeling Density-Driven Flow in Porous Media, Springer, Heidelberg / New York. 286 p.

Holzbecher, E. and Kohfahl, C. (2008). Geothermic modelling using COMSOL multiplysics-manual course. Freie Universität Berlin. 56 p.

Hsieh P.A. and Winston R B. (2002). User´s guide to model viewer, a program for three-dimensional visualization of ground-water model results. Report 02-106, U.S. Geological Survey, Water resources Investigations.

Kangas M.T.and Lund P.D. (1995). THETA - An Advanced Simulation Program for 3D Fluid, Heat, and Solute Transfer in Porous Media. Helsinki University of Technology, Report TKK-F-A732, 120 p.

Kipp, K.L. (1986). HST3D – A computer code for simulation of heat and solute transport in 3D ground water flow systems. Report 86-4095, U.S. Geological Survey, Water resources Investigations.

Kohl T. and Hopkirk R.J. (1995). FRACTure- A simulation code for forced fluid flow and transport in fractured, porous rock. Geothermics, vol. 24, issue 3, p. 333-343.

Kolditz, O, Habbar, A., Kaiser, R., Rother, T., Thorenz, C., Kohlmeier, M. and Moenickes, S. (2001). ROCFLOW user´s manual release 3.5. Institute of fluid mechanics and computer applications in civil engineering. University of Hannover.

Kühn M. (2004). Reactive flow modelling of hydrothermal systems. Springer. Berlin-Heidelberg, 261 p.

Langevin C.D., Thorne, Jr, D., Dausman A.M., Sukop, Michael D. and Weixing G. (2007). SEAWAT version 4: A computer program for simulation of multi-species solute and heat transport. U.S. Geological Survey Techniques and method book 6, chapter A22, 39 p.

Loague, K. and Green, R. E. (1991). Statistical and graphical methods for evaluating solute transport models: Overview and application, J. Contaminant Hydrology, 7, p. 51-73.

Lund John W., Derek H. Freeston, and Boyd T.L. (2005). Direct Application of geothermal energy: 2005 Worldwide review. Geothermics, vol. 34, issue 3, p. 691-727.

Marsily, G. (1986). Quantitative Hydrogeology, Academic Press, Orlando.

Molina G., N (2008). Verification of MT3DMS as heat transport code using analytical solutions. Master thesis. Centre for Applied Geosciences (ZAG). University of Tübingen. Germany.

O´Sullivan Michael J., Karsten Pruess and Lippmann, M. (2000). Geothermal reservoir simulation: The state of the practice and emerging trends. Proceedings World Geothermal Congress 2000, Japan.

Pape H., Clauser, C., Iffland, J., Krug, R and Wagner, R. (2005). Anhydrite cementation and compaction in geothermal reservoirs: Interaction of pore space structure with flow, transport, P-T conditions, and chemical reactions. International Journal of Rock Mechanics and Mining Sciences, vol. 42, issues 3-4, p. 1056-1069.

Pejman R. (2008). Numerical Verification of Shallow Geothermal Models Using FEFLOW. Master thesis. Centre for Applied Geosciences (ZAG). University of Tübingen. Germany.

Pruess, K. Oldenburg, C. and Moridis, G. (1996). THOUGH2 User's Guide, Version 2.0, Lawrence Berkeley National Laboratory Report LBL-38383, SN027.

Rühaak W., Rath, V., Wolf, A. and Clauser, C. (2008). 3D finite volume groundwater and heat transport modeling with non-orthogonal grids, using a coordinate transformation method. Advances in Water Resources, vol. 31, issue 3, p. 513-524.

Schmidt, T and Hellström G. (2005). Ground source cooling - working paper on usable tools and methods. EU Commission SAVE Programme and Nordic Energy Research. 21 p.

VDI (Association of German Engineers) (2000). Thermal use of the underground. VDI-4640 first part. Beuth Verlag GmbH, Berlin. 32 p.

Zheng C. (2006). MT3DMS V 5.2 Supplementary guide. Technical report, Department of geological sciences, University of Alabama. 46 p.

Zheng, C and Bennett G. (1995). Applied contaminant transport modelling. International Thomson publishing Inc. 433 p.

Zheng, C. and Wang P.P. (1999). MT3DMS: A modular three-dimensional multispecies model for simulation of advection, dispersion and chemical reactions of contaminants in groundwater systems; Documentation and User's Guide, Contract Report SERDP-99-1, U.S. Army Engineer Research and Development Center, Vicksburg, MS.

7 APPENDIX

Input file example for 2D scenario with the following features:

- Grid size: 400 m × 400 m
- Confined aquifer
- Gradient i=4.0E-4
- Energy extraction 60 W

Some input parameters are not explained in the following descriptions. Information about them can be found in the respective user´s manuals (MODFLOW: Harbaugh et al., 2000, pages 41-88; MT3DMS: Zheng and Wang, 1999, pages 102-127)

INPUT FILES FOR MODFLOW 2000

NAME FILE: *flowmodel.nam*

Package(UN)	File name	Description
LIST 6	*flowmodel.lst*	List file (all results are saved in this file)
BAS6 5	*flowmodel.ba6*	Basic package
BCF6 7	*flowmodel.bc6*	Block centered flow package
DIS 10	*flowmodel.dis*	Discretization package
PCG 11	*flowmodel.pcg*	Preconditionated conjugate-gradient package (solver)
FHB 12	*flowmodel.fhb*	Flow and head boundary package
LMT6 66	*flowmodel.lmt*	Link-MT3DMS package
DATA 50	*flowmodel.geo*	Input data: boundary conditions
DATA 52	*flowmodel.hea*	Input data: Initial hydraulic heads
OC 14	*flowmodel.out*	Output control package
DATA 53	*head.sal*	Output data: hydraulic heads
DATA 54	*flow.sal*	Output data: volumetric flow
DATA 55	*icb.sal*	Output data: boundary conditions
DATA(binary) 56	*budg.sav*	Output data: water flow budget
DATA 15	*delr.in*	Input data: row discretization
DATA 16	*delc.in*	Input data: column discretization

UN: unit number

BASIC PACKAGE: *flowmodel.ba6*

```
#1 LAYER CASE, 2D, 400 ROWS, 402 COLUMNS; STEADY STATE
#CONFINED AQUIFER
FREE                          Input format for all packages (no space sensitive)
EXTERNAL 50  1  (FREE) -1     Bounday condition (external file, UN=50,flowmodel.geo)
999.99                        Head for inactive cells
CONSTANT  2.0                 Initial hydraulic head for all the cells
```

BLOCK CENTERED FLOW PACKAGE: *flowmodel.bc6*

```
56 5.0 0 0.0 0 0              Flow budget file UN and wett capability (deactivated)
00                            Layer type (confined)
CONSTANT 1.0                  Anysotropy factor (isotropic)
CONSTANT 8.0E-3               Transmisivity [m s⁻¹]
```
(where "Transmisivity [m s^{-1}]")

DISCRETIZATION PACKAGE: *flowmodel.dis*

```
   1 400 402  1 1 2                Number of layer, columns, rows and periods. Unit [s, m]
 0                                 No confining bed
EXTERNAL  15  1  (free) -1         Row discretization (external file, delr.in)
EXTERNAL  16  1  (free) -1         Column discretization (external file, delc.in)
CONSTANT   1.0                     Elevation layer [m]
CONSTANT   0.0                     Bottom elevation of the layer
 6912E+4  1  1.000E+00  SS         Period leght [s], number stress periods, Steady state
```

PRECONDITIONED CONJUGATE-GRADIENT PACKAGE: *flowmodel.pcg*

```
90 20 1                            Outter, inner iterations
5.0E-5 1.0E-6 1.0 2 2 0 1.0        Head change, and error convergence criterion
```

FLOW AND HEAD BOUNDARY PACKAGE: *flowmodel.fhb*

```
1 0 800 0 0 0 0                    Times when head are assigned, number of cells
12  1.0 1                          Unit number of the flow and heat boundary file
0.0                                Multiplier
52  1.0 1                          Initial heads file (UN 52: flowmodel.hea)
```

LINK-MT3DMS PACKAGE: *flowmodel.lmf*

```
OUTPUT_FILE_NAME path: flowmodel.ftl      Path where link file is saved (also file name)
OUTPUT_FILE_UNIT 20                       Link file unit number
OUTPUT_FILE_HEADER extended               Link file header
OUTPUT_FILE_FORMAT unformatted            Link file format (binary)
```

OUTPUT CONTROL PACKAGE: *flowmodel.out*

```
# Output control for the flow simulation
HEAD SAVE FORMAT (25F10.3) LABEL
HEAD SAVE UNIT 53
DRAWDOWN SAVE FORMAT (25F10.3) LABEL
DRAWDOWN SAVE UNIT 54
IBOUND SAVE FORMAT (500I2) LABEL
IBOUND SAVE UNIT 55
PERIOD 1 STEP 1
SAVE HEAD
SAVE DRAWDOWN
SAVE BUDGET
```

INPUT FILES FOR MT3DMS

MT3DMS input files are sensitive to the number of blanks, generally ten blanks between values are necessary.

NAME FILE: *heatmodel.nam*

Package(UN)		File name	Description
LIST	0	heatsim.lst	List file (all results are saved in this file)
BTN	0	heatsim.btn	Basic transport package
ADV	0	heatsim.adv	Advection package
DSP	0	heatsim.dsp	Dispersion package
SSM	0	heatsim.ssm	Sink and source mixing package
RCT	0	heatsim.rct	Chemical reaction package

GCG	0		heatsim.gcg			Generalized conjugate gradient solver package
FTL	0		flowmodel.ftl			Input data: flow model link file
DATA	30		heatsim.con			Input data: boundary conditions
DATA	22		alpha.in			Input data: longitudinal dispersivity
DATA	23		diff.in			Input data: thermal diffusion
DATA	52		delr.in			Input data: row discretization
DATA	53		delc.in			Input data: column discretization

BASIC TRANSPORT PACKAGE: *heatsim.btn*

```
#2D HEAT TRANSPORT IN UNIFORM FLOW FIELD WITH CONTINUOUS POINT SOURCE
#CONFINED ACUIFER
```

1	402	400	1	1	1	Number of layers, rows, columns, stress periods and species
S M KG						Units
T T T T T F F F F F						Used packages (ADV, DSP, SSM, RCT and GCG)
0						Type of layer (confined)
0	1.0					Row discretization
0	1.0					Columns disccretization
0	1.0					Top elevation in first layer
0	1.0					Thickness of each layer
0	.26					Effective posority
30	1	(400I2)	-1			Boundary condition (external file, UN=30)
0	285.15					Initial temperature [k]
-1E10	0.01					Temperature at inactive cells
0	0	0	0	T		Results saving instruction
6						Number of times at which results are saved in obs. file
864E+3	1728E+3	3456E+3	6912E+3	6048E+4	6912E+4	Total elapsed time at which results are saved
200	1000					Number of observation points and frequency
1	201	20				
	.					Location of obs. points, layer, row and column
	.					
1	201	219				
F	1					Mass balance information
6912E+4	1	1.				Stress period length, number time steps, multiplier
0.	10000	1.	0.0			Step size (auto), Max. number of transport steps

ADVECTION PACKAGE: *heatsim.adv*

-1	1	Third order TVD (ULTIMATE) solver, Courant num.

DISPERSION PACKAGE: *heatsim.dsp*

$ multidiffusion				Multidiffusion option activated
22	1	(400F4.2)	-1	Input file: longitudinal dispersivity, UN= 22
0	0.01			Ratio of horizontal transverse dispersivity to longitudinal dispersivity
0	0.01			Ratio of vertical transverse dispersivity to longitudinal dispersivity
23	1	(400E7.2)	-1	Input file: thermal diffusivity, UN=23

SINK AND SOURCE MIXING PACKAGE: *heatsim.ssm*

T F F F F F F F F F					Sink/source option, only well is activated
1001					Max. number of sink/source points
1					Number of point sources
1	201	20	-1.43E-5	15	Location of point source, layer, row, column, mass

loading rate and type of source (mass load)

CHEMICAL REACTION PACKAGE: *heatsim.rct*

1	0	2	0	Linear isotherm, no kinetic reaction, variables are 3D arrays, initial concentration for sorbed phases is not read
0	1961.			Bulk density of the aquifer medium [kg m^{-3}]
0	2.103e-4			Distribution coefficient [m^3 kg^{-1}]
0	2.			Read but not used parameter

GENERALIZED CONJUGATE GRADIENT SOLVER PACKAGE: *heatsim.gcg*

100	40	1	1	Outter and inner iterations
1.0	1E-6	0		Relaxation factor, convergence criterion